Simulation of cable coupling Final Report

David W. P. Thomas

January, 2009

Abstract

This is the final report conducted during my study period in Thales, Nederland form September 2008 to January 2009. The work was focussed on the study of cable coupling. This has involved developing models of the cable coupling phenomenon and developing some statistical analysis. Results show that the estimate cable coupling compares reasonably well with measurements and the statistical analysis provides some useful bounds for the expected values and insight into the important parameters. From a comparison of the braid transfer impedance models it is concluded that the Kley model seems reasonably accurate. From the measurement results provided by previous Thales reports it is apparent that stray reactances play an important role in defining the resonant points in the cable coupling. Comparable simulation results can be obtained through the application of reasonable stray reactive values. At resonance the cable coupling will only be limited by losses in the circuit and this can provide a simple estimate of the maximum cable coupling. Using an estimate of the losses and the statistical distribution of the important parameters provides an engineer with the probability distribution of the cable coupling. A full description of the approach and the advantages it provides for efficient and cost effective EMC compliance is given in this report.

Contents

1 Theory of cable transfer impedance **2**
- 1.1 Sheath parameters . . . 2
- 1.2 Vance model . . . 3
- 1.3 Tyni model . . . 4
- 1.4 Kley model . . . 5
- 1.5 Braid internal impedance for external propagation . . . 6
- 1.6 Double braided cables . . . 6

2 Theory of cable coupling via the braid transfer impedance **7**
- 2.1 High frequency cable coupling . . . 11

3 Statistical analysis and the application of Unscented Transforms **14**
- 3.1 Statistical parameters . . . 14
- 3.2 The Unscented Transform (UT) . . . 15
  - 3.2.1 Calculation of the sigma points . . . 15
  - 3.2.2 Calculation of the moments of the mapped distribution . 17
  - 3.2.3 Accuracy of the unscented transform . . . 18
  - 3.2.4 The multivariate Unscented Transform . . . 19
  - 3.2.5 Estimation of a variables influence in the multivariate case . . . 19

4 Results **20**
- 4.1 Comparison of the transfer impedance models . . . 20
  - 4.1.1 Single braided cables . . . 20
  - 4.1.2 Double braided cables . . . 22
- 4.2 Predicted and measured cable coupling . . . 34
  - 4.2.1 Single braided cable (RG58) . . . 36
  - 4.2.2 Double braided cable (RG214) . . . 47
- 4.3 Prediction of the peak cable coupling . . . 51
- 4.4 Statistical analysis of the cable coupling . . . 55

5 Conclusions **69**

1 Theory of cable transfer impedance

In this section three well known models for cable transfer impedance were considered and compared for cable sheaths with a single layer weave. The models considered were the models of Vance [1], Tyni [2], and Kley [3]. Note that in the past different nomenclatures have been used for describing the models so a table is provided in the appendix comparing the nomenclature used in this report with previous work.

1.1 Sheath parameters

The basic parameters of a braided sheath as depicted in Figure 1. are:

P Picks or the number of carrier crossings per unit length

N Number of carriers

n Number of wires in each carrier

l lay length (one carrier rotation)

d wire diameter

α braid angle

h radial spindle separation.

D_o outer diameter of dielectric

D_m mean braid diameter

b hole width

The above parameters over specify the braid, so P or l are given as and the other parameter is deduced from:

$$l = \frac{N}{2P} \tag{1}$$

Braid angle α and radial spindle separation h are also calculated from (2), (3) and (4) as proposed by Katakis [4] who suggested D_m is also a function of h. The equations represent a non-linear relationship so a solution is found through a Newton-Raphson iteration of the equations.

$$\tan\alpha = \frac{2\pi D_m P}{N} \tag{2}$$

$$\left[\frac{2\pi}{N}\cos\alpha\right] h^2 + \left[(1-n)d + \frac{2\pi}{N}(D_o + 2d)\cos\alpha\right] h - 2d^2 = 0 \tag{3}$$

$$D_m = D_o + 2d + h \tag{4}$$

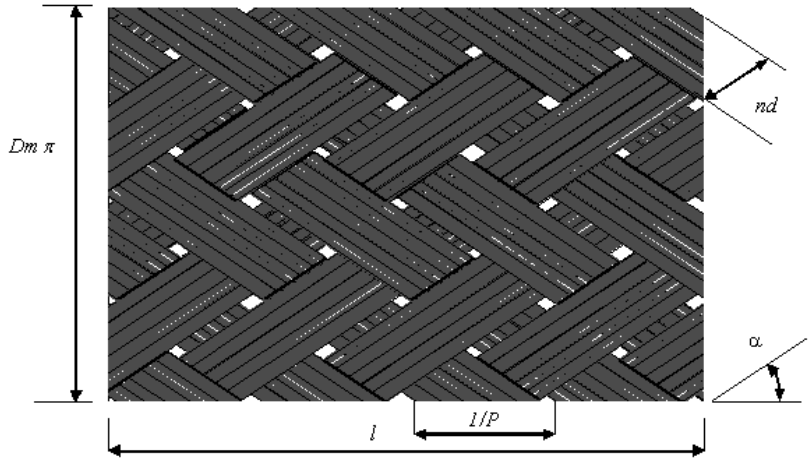

Figure 1: Detail of the sheath showing defined parameters (m=8, n=5)

Once h and $alpha$ are found then

$$b = \frac{2\pi D_m}{N}\cos\alpha - nd \tag{5}$$

These then are all the parameters necessary to define the shield for the calculation of the transfer impedance. A typical set of cable parameters can be found in [5].

1.2 Vance model

The Vance model [1] is one of the earliest and simplest models which takes into account skin depth and braid inductance. The DC resistance of the braid is given by

$$R_c = \frac{4}{\pi d^2 n N \sigma \cos\alpha} \tag{6}$$

Then allowing for the skin depth effect the screen impedance can be found from [5]

$$Z_d = R_c \frac{(1+j)d/\delta}{\sinh((1+j)d/\delta)} \tag{7}$$

where the skin depth $\delta$is given by

$$\delta = \frac{1}{(\pi f \mu_0 \sigma)^{1/2}} \tag{8}$$

Additionally to the screen impedance is a braid inductance M which is given by

$$M = \frac{\pi \mu_0}{6N}(1-\chi)^{3/2}\frac{e^2}{E(e)-(1-e^2)K(e)} \tag{9}$$
$$e = (1-\tan^2\alpha)^{1/2} \quad \text{if} \quad \alpha < 45^o$$

or

$$M = \frac{\pi \mu_0}{6N}(1-\chi)^{3/2}\frac{\frac{e^2}{\sqrt{1-e^2}}}{E(e)-(1-e^2)K(e)} \tag{10}$$
$$e = (1-\cot^2\alpha)^{1/2} \quad \text{if} \quad \alpha > 45^o$$

where $K(e)$ and $E(e)$ are complete elliptic integrals of the first and second kind, respectively, defined by

$$K(e) = \int_0^{\pi/2} \frac{d\varphi}{(1-e^2\sin^2\varphi)^{1/2}} \tag{11}$$

$$E(e) = \int_0^{\pi/2} (1-e^2\sin^2\varphi)^{1/2} d\varphi \tag{12}$$

F is fill factor of braid given by

$$F = \frac{nNd}{2\pi D_m \cos\alpha} \tag{13}$$

F_0 is the minimal filling factor given by

$$F_0 = F\cos\alpha \tag{14}$$

and the optical coverage χ is given by

$$\chi = 2F - F^2 \tag{15}$$

The total transfer impedance is then given by

$$Z_T(f) = Z_d(f) + 1j\omega M \tag{16}$$

1.3 Tyni model

In the Tyni model [2] the transfer impedance is found from the braid inductance L_b and the leakage or gap inductance L_h due to the gaps in the screen. This model was studied extensively in [8] and found to be reasonably accurate.

$$L_b = \frac{\mu_0 h}{4\pi D_m}(1 - tan^2\alpha) \tag{17}$$

$$L_h = \frac{\mu_0 2N}{\pi cos\alpha}\left(\frac{b}{\pi D_m}\right)^2 exp\left(\frac{-\pi d}{b} - 2\right) \tag{18}$$

Note that the equation for L_b is as quoted by Benson et al. [8] but this appears to be different to that quoted in the Thales report [7] The transfer impedance Z_t is then given by

$$Z_t = Z_d + j\omega(L_h - L_b) \tag{19}$$

where Z_d is the braid impedance allowing for skin depth given by 7

1.4 Kley model

The Kley model [3]is the best and most rigorously developed of the three models and the Thales report 3.3 RCTR study [7]suggests that this is probably the more accurate.

In the Kley model there are inductances; M_l due to the apertures allowing for the curvature of the screen, M_g mutual inductance between carriers in the braid and and an inductive term due L_s to the tangential components of the electromagnetic field.

These inductances are given by the following equations

$$M_l = 0.875M\exp(-\tau_h) \tag{20}$$

$$M_g = \frac{-0.11}{Nn}\mu_0\cos(2K_1\alpha) \tag{21}$$

$$L_s = \frac{1}{\omega\pi\sigma\delta}[D_l^{-1} + D_g^{-1}] \tag{22}$$

where M is given by 10 and

$$\tau_h = 9.6F\sqrt[3]{\chi^2 d/D_m} \tag{23}$$

$$K_1 = \frac{\pi}{4}\left[\frac{2}{3}F_0 + \frac{\pi}{10}\right] \tag{24}$$

$$D_l^{-1} = \frac{10\pi F_0^2\cos\alpha}{D_m}[1 - F]\exp(-\tau_E) \tag{25}$$

$$D_g^{-1} = \frac{-3.3}{2\pi F_0 D_m}\cos(2K_2\alpha) \tag{26}$$

$$\tau_F = 12F\sqrt[3]{\chi^2 d/D_m} \tag{27}$$

$$K_2 = \frac{\pi}{4}\left[\frac{2}{3}F_0 + \frac{3}{8}\right]^{-1} \tag{28}$$

The total transfer impedance is then given by

$$Z_t = Z_d + j\omega(M_l + M_g + L_s) \tag{29}$$

Kley also found that better results were obtained if the braid wire diameter d was replaced by an adjusted value d_r given by

$$d_r = \frac{0.67d}{\sqrt{\cos\alpha}} \tag{30}$$

1.5 Braid internal impedance for external propagation

As well as providing a transfer mechanism between the internal voltages and currents and the external voltage and currents it also forms the transmission line conductor for the internal and external propagation. The internal impedance of the braid conductor for the external propagation is an important parameter because it provides one of the main loss mechanisms for the external circuit. From [5] the internal impedance for the external circuit of a cylindrical conductor is

$$Z_e = \frac{1}{\pi D_m \sigma d}\frac{(1+j)d}{\delta}\coth\frac{(1+j)d}{\delta} \approx R_c\frac{(1+j)d}{\delta}\coth\frac{(1+j)d}{\delta} \tag{31}$$

This may be further adjusted to allow for a non uniform distribution of the external surface current due to the nature of the external circuit.

1.6 Double braided cables

There is a wide range of multiple shielded cables but in this work the transfer impedance of a double braid which is periodically connected together at electrically short spacings as found in cable RG214 was investigated. For this type of cable braid a transfer impedance can be derived which can be treated in the same way as a single braid. The equivalent transfer impedance for a two-layer braid periodically shorted together is given by [5]

$$Z_t = \frac{Z_{T1}Z_{T2}}{Z_{i1} + Z_{i2} + j\omega L_{12}} \tag{32}$$

where Z_{i1} = inner impedance of the inner shield given by 31 , Z_{i2} = inner impedance of the outer shield given by 31 , Z_{T1} The transfer impedance of the inner shield, Z_{T2} The transfer impedance of the outer shield and L_{12} is the inductance of the shield to shield transmission line given by

$$L_{12} = \frac{\mu_0}{2\pi}\ln\frac{a_2}{b_1} \tag{33}$$

with b_1 is the inner braid outer radius and a_2 is the outer braid inner radius.

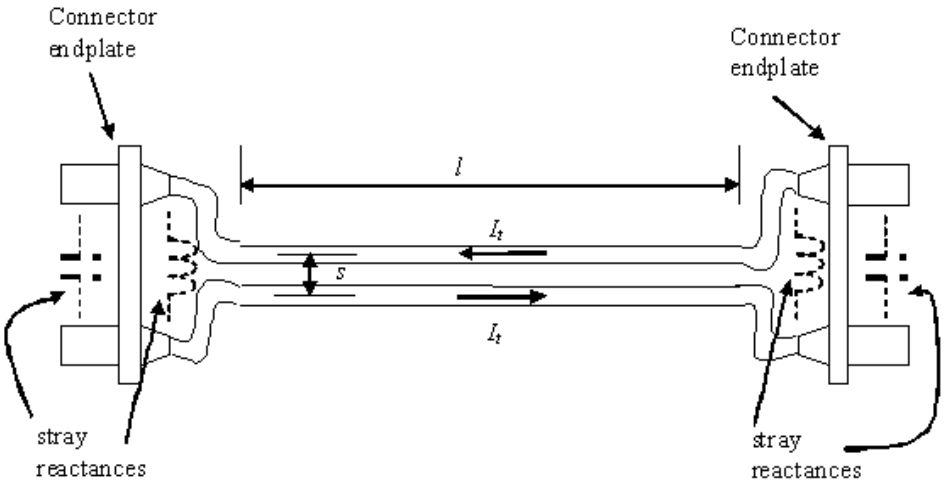

Figure 2: A typical cable layout of two parallel cables showing points were significant stray reactances can affect coupling

2 Theory of cable coupling via the braid transfer impedance

In this work the cable coupling due to transfer impedance alone is considered. The effect of transfer admittance has not been included as for non optimized cable sheaths it should only have a small effect [9, 10]. Coupling due to the effect of a transfer impedance will occur between cables when they are laid roughly in parallel along a common path. A typical cabling arrangement is shown in Figure 2 where the cables have approximately a constant separation along a length l, for instance due to being laid in cable trunking, but the cables normally diverge near their connection points. The nature of the terminations strongly effects the degree of cable coupling at high frequencies due to the stray reactances they introduce. If the cables are connected to a common connector endplate (or common cabinet) then the stray reactance will be inductive due to the introduction of an extra loop area, but if the cables are connected to electrically isolated units then the stray reactance will be mostly capacitive. These stray reactances at the terminations can only be estimated due to the geometric complexity of the terminations and the lack of known details. The terminations are therefore the main limit to the accuracy to which the cable coupling can be predicted.

The equivalent circuit for the coupling path created by the cable sheath transfer impedance is shown in Figure 3. The currents I_s along the source cable

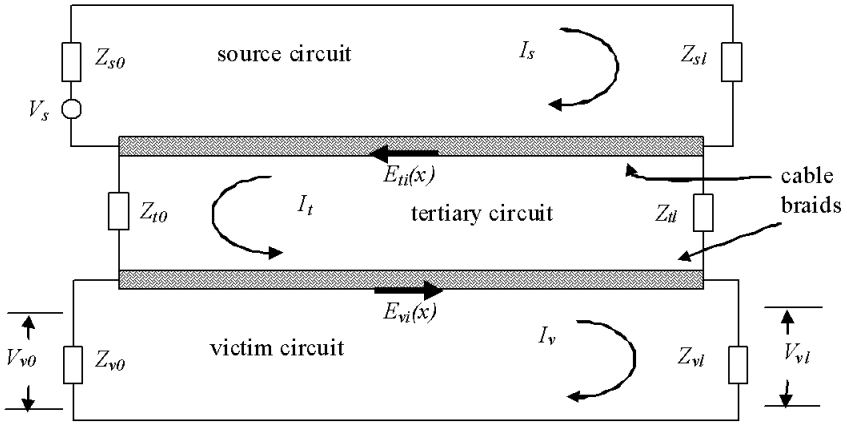

Figure 3: Equivalent circuit for cable coupling between two shielded cables via the shield transfer impedance

creates a voltage gradient $E_{it}(x)$ along the outer sheath given by

$$E_{it}(x) = Z_{ts} I_s(x) \tag{34}$$

where Z_{ts} is the shield transfer impedance of the source cable and x is the distance along the cable sheath. The voltage gradient on the source cable will then induce a current on the outer sheath of the victim cable. This induced current circulates around a circuit composed of the outer sheaths of the two parallel cables and termed the tertiary circuit. For low frequencies ($\lambda >>$ the length of the cables) the sheath voltage gradient is independent of x. The equivalent circuit for low frequency coupling to a transmission line is as given in Figure 4. the induced current in the tertiary circuit I_t is then given by

$$I_t = \frac{E_{it} l}{j\omega L_{tl} l + Z_{t0} + Z_{tl}} = \frac{Z_{ts} I_s l}{j\omega L_{tl} l + Z_{t0} + Z_{tl}} \tag{35}$$

where $\omega = 2\pi f$ is the angular frequency , L_t is the inductance per unit length of the tertiary cable pair, Z_{t0} and Z_{tl} are the termination impedances at each end of the tertiary circuit (i.e. they represent the termination stray reactances in parallel with half the total transmission line capacitance) and l is the length over which the cables are approximately parallel. For cables laid closely together $\omega L_{tl} l$ may be comparable to Z_{t0} and Z_{tl} and hence the difficulty in estimating the cable coupling.

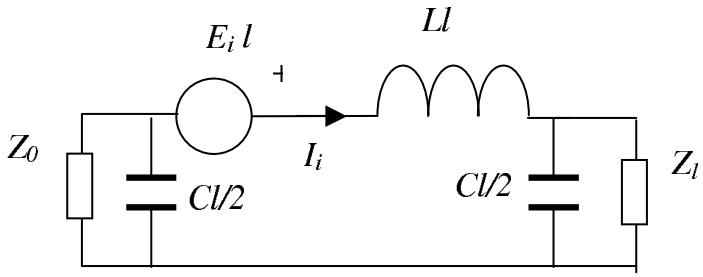

Figure 4: Equivalent circuit for low frequency cable coupling

The induced tertiary current will in turn induce a current I_v in the victim cable due to the induced voltage gradient $E_{vi}(x)$ caused by the victims sheath transfer impedance Z_{tv}, as shown in Figure 3. The induced victim current will then creates a voltage across the terminations of the victim cable which is the usual measurable form of the cable coupling. For example the voltage across terminal 0 of the victim V_{v0} will be given by

$$V_{v0} = \frac{Z_{tv} I_t l Z_{v0}}{Z_{v0} + Z_{vl}} = \frac{Z_{tv} Z_{ts} I_s l^2 Z_{v0}}{(Z_{v0} + Z_{vl})(j\omega L_{tl} l + Z_{t0} + Z_{tl})} \tag{36}$$

where Z_{v0} and Z_{vl} are the termination impedances of the victim circuit.

The cable coupling is then quantified by the ratio of the received victim voltage to the source voltage. The coupling C in dB is then defined as

$$C = 20 \log_{10} \left(\frac{V_{v0}}{V_s} \right) \tag{37}$$

The current in the tertiary circuit is often called the common mode current but in fact it has the form of a differential mode as the victim and source currents are of opposite sign. The presence of another cable or a ground plane will enable other current paths to form and reduce the coupling between two cables. In the case of an additional ground plane the induced tertiary circuit current would have two modes of the form of a differential and common mode. The general equivalent coupling circuit for two cables above a ground plane can be represented by the circuit given in Figure 5. The differential and common

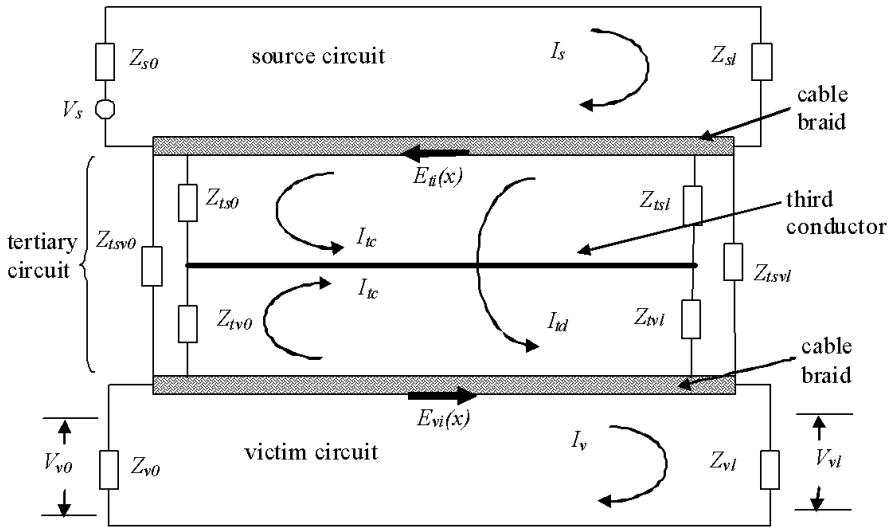

Figure 5: Equivalent circuit for cable coupling between two shielded cables via shield transfer impedance in the presence of a third conductor (ground plane of third cable shield)

mode currents (I_{td} and I_{tc}) on the cable sheaths are related to the total sheath currents on the source cable and victim cable (I_{ts} and I_{tv} respectively) by

$$\begin{bmatrix} I_{ts} \\ I_{tv} \end{bmatrix} = \begin{bmatrix} -1 & 1 \\ 1 & 1 \end{bmatrix} \begin{bmatrix} I_{td} \\ I_{tc} \end{bmatrix} \tag{38}$$

or

$$[I_{tsv}] = [S][I_{tcd}] \tag{39}$$

where $[I_{tsv}]$ is the vector of cable sheath currents, $[I_{tcd}]$ is the vector of common mode and differential mode currents and $[S]$ is the modal transformation matrix. For low frequencies ($\lambda >>$ the length of the cables) the induced common mode and differential mode currents on the tertiary circuit cable sheaths are then related to the source sheath voltage ($E_{ti}l$) by

$$\begin{bmatrix} E_{ti}l \\ 0 \end{bmatrix} = \left(j\omega l \begin{bmatrix} L_{ts} & L_{tm} \\ L_{tm} & L_{tv} \end{bmatrix} + [Z_{t0}] + [Z_{tl}] \right) \begin{bmatrix} I_{ts} \\ I_{tv} \end{bmatrix} \tag{40}$$

where L_{ts} and L_{tv} are the self inductance of the source and victim shields respectively, L_{tm} is the mutual inductance between the source and victim cable shields, $[Z_{t0}]$ and $[Z_{tl}]$ are the impedance matrices of the tertiary circuit terminations as depicted in figure 5 and these then have the form

$$[Z_{tX}] = \begin{bmatrix} \frac{Z_{tsx}(Z_{tvx}+Z_{tsvx})}{Z_{tsvx}+Z_{tsx}+Z_{tvx}} & \frac{Z_{tsx}Z_{tvx}}{Z_{tsvx}+Z_{tsx}+Z_{tvx}} \\ \frac{Z_{tsx}Z_{tvx}}{Z_{tsvx}+Z_{tsx}+Z_{tvx}} & \frac{Z_{tvx}(Z_{tsx}+Z_{tsvx})}{Z_{tsvx}+Z_{tsx}+Z_{tvx}} \end{bmatrix} \tag{41}$$

where $X = 0$ or l

Equation (40) is then solved for the victim current I_{tv} which can then be substituted for I_t in (36) to find the induced voltage across the victim termination/connector.

For higher frequencies the voltage per unit length along the source cable sheath will have a significant variation along the cable length due to propagation effects and these need to be taken into account. The propagation effects lead to resonances in the tertiary circuit and a significant increase in cable coupling.

2.1 High frequency cable coupling

For high frequencies the cable currents are no longer uniform and the propagation effects have to be considered. For a general source cable with supply impedance Z_{s0} and load impedance Z_{sl} the the input current $I_s(0)$ at the supply connector is related to the supply voltage V_s by

$$I_s(0) = \frac{V_s}{Z_{s0} + Z_c \left[\frac{Z_{sl} + Z_c \tanh \gamma_s l}{Z_c + Z_{sl} \tanh \gamma_s l}\right]} \tag{42}$$

where Z_c is the characteristic impedance of the source cable (i.e. typically 50 Ω) and γ_s is the propagation constant of the cable (i.e. $\gamma_s \approx j\omega/u$ where u is typically 2c/3). The current can also be defined in terms of forward and backward propagating waves such that

$$I_s(0) = I_s^+ + I_s^- = I_s^+ + \rho_{is} I_s^+ \tag{43}$$

where

$$\rho_{is} = \left[\frac{Z_c - Z_{sl}}{Z_{sl} + Z_c}\right] e^{-2\gamma_s l} \tag{44}$$

Thus (42) and (43) can be combined to give

$$I^+ = \frac{[Z_c + Z_{sl}] e^{\gamma_s l} V_s}{2[Z_{sl}(Z_c \cosh \gamma_s l + Z_{sl} \sinh \gamma_s l) + Z_c(Z_{sl} \cosh \gamma_s l + Z_c \sinh \gamma_s l)]} \tag{45}$$

The current along the source cable is then given by

$$I_s(x) = [e^{-\gamma_s x} + \rho_{is} e^{\gamma_s x}] I^+ \tag{46}$$

where x is the distance along the cable from the supply point. The voltage gradient along the shield of the source cable is then also a function of x as given by

$$E_{ti}(x) = Z_{ts} I_s(x) \tag{47}$$

The cable sheath tertiary circuit and the victim cable will be equivalent to transmission lines with a distributed series voltage source of the form as shown in the line section given in Figure 6. The differential equations describing the

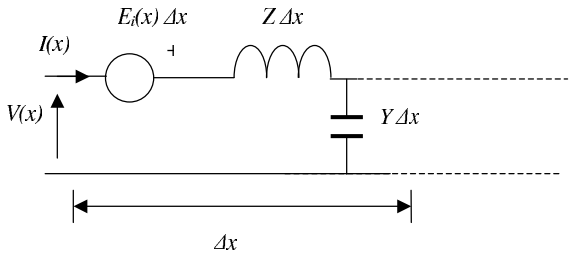

Figure 6: Equivalent circuit a section Δx of a transmission line with a distributed series voltage source.

induced voltagesV_i and currents I_i on transmission lines with a distributed series voltage source $E_i(x)$ are given by Vance [5].

$$\frac{\partial V_i}{\partial x} = E_i(x) - I_i Z \tag{48}$$

$$\frac{\partial I_i}{\partial x} = -YV_i \tag{49}$$

where Z and Y are the transmission line series impedance and shunt admittance respectively. Equations (48) and (49) can be differentiated and combined to give

$$\frac{\partial^2 V_i}{\partial x^2} - \gamma^2 V_i = \frac{\partial E_i(x)}{\partial x} \tag{50}$$

$$\frac{\partial^2 I_i}{\partial x^2} - \gamma^2 I_i = -YE_i(x) \tag{51}$$

Equation (51) has a general solution of the form [5] :

$$I_i(x) = [K_1 + P(x)]e^{-\gamma x} + [K_2 + Q(x)]e^{\gamma x} \tag{52}$$

where

$$P(x) = \frac{1}{2Z_c}\int_0^x e^{\gamma u} E_i(u)du \tag{53}$$

$$Q(x) = \frac{1}{2Z_c}\int_x^l e^{-\gamma u} E_i(u)du \tag{54}$$

and K_1 and K_2 are set to satisfy the boundary conditions at $x = 0$ and $x = l$ which gives

$$K_1 = \rho_1 \left[\frac{\rho_2 P(l)e^{-\gamma l} - Q(0)e^{\gamma l}}{e^{\gamma l} - \rho_1\rho_2 e^{-\gamma l}}\right] \tag{55}$$

$$K_2 = \rho_2 e^{-\gamma l}\left[\frac{\rho_1 Q(0) - P(l)}{e^{\gamma l} - \rho_1\rho_2 e^{-\gamma l}}\right] \tag{56}$$

where $Z_c = \sqrt{Z/Y}$, $\gamma = \sqrt{ZY}$ and

$$\rho_1 = \frac{Z_0 - Z_c}{Z_0 + Z_c} \tag{57}$$

$$\rho_2 = \frac{Z_l - Z_c}{Z_l + Z_c} \tag{58}$$

Equation (52) is therefore used to first find the currents induced on the tertiary cable sheath circuit and then it is also applied to the victim cable using the deduced tertiary current profile to deduce the induced victim current and the voltage induced across the victim terminals using.

$$V_{v0} = Z_{v0} I_{vi}(0) \tag{59}$$

$$V_{vl} = Z_{vl} I_{vi}(l) \tag{60}$$

For multiple cables or cables in the presence of a ground plane the currents induced on each of the cable sheaths will be different and the governing equations will comprise of N simultaneous equations where $N =$ the number of cables in the presence of a ground plane or $N + 1$ is the total number of cables when a ground plane is not present. The governing equations are then

$$\left[\frac{\partial^2 V_i}{\partial x^2}\right] - [Z][Y][V_i] = \left[\frac{\partial E_s(x)}{\partial x}\right] \tag{61}$$

$$\left[\frac{\partial^2 I_i}{\partial x^2}\right] - [Y][Z]\,[I_i] = -\,[Y]\,[E_i(x)] \tag{62}$$

where [X] represents now a vector of the N components of X. Equations (61) and (62) therefore represent N simultaneous equations. However if we transform the components into model components using

$$[X_m] = [S]^{-1}[X] \tag{63}$$

where $[S]$ is the transformation matrix comprising of the eigen vectors of $[Y][Z]$ then (62) has the form of N independent equations

$$\left[\frac{\partial^2 I_{im}}{\partial x^2}\right] - [\gamma_m]^2\,[I_i] = -[S]^{-1}\,[Y]\,[S]\,[E_{im}(x)] \tag{64}$$

where $[\gamma_m]^2$ is a diagonal matrix of the eigen values of $[Y][Z]$ and the general solution is of the form:

$$[I_i(x)] = [[K_1] + [P(x)]][e^{-\gamma x}] + [[K_2] + [Q(x)]][e^{\gamma_m x}] \tag{65}$$

where

$$[K_1] = [\rho_1]([e^{\gamma l}] - [\rho_1][\rho_2][e^{-\gamma l}])^{-1}([\rho_2][P(l)][e^{-\gamma l}] - [Q(0)][e^{\gamma l}]) \tag{66}$$

$$[K_2] = [\rho_2][e^{-\gamma l}]([e^{\gamma l}] - [\rho_1][\rho_2][e^{-\gamma l}])^{-1}([\rho_1][Q(0)] - [P(l)]) \tag{67}$$

where

$$[\rho_1] = ([Z_0] + [Z_c])^{-1}([Z_0] - [Z_c]) \quad \rho_2 = ([Z_l] + [Z_c])^{-1}([Z_l] - [Z_c]) \tag{68}$$

where $[Z_0]$ and $[Z_l]$ are given by 42.

3 Statistical analysis and the application of Unscented Transforms

The nature of Electromagnetic compatibility (EMC) involves process the parameters of which are often only poorly known or can have a significant variation. Uncertainty is one of the most challenging aspects of EMC analysis. This is particularly true for cable coupling where it is found that the properties of the external circuit strongly effects the degree of coupling experienced. The parameters of the external circuit depends on the installation of the cables which can only be known to a certain accuracy or may vary in a random fashion.Therefore cable coupling can only be quantified within certain statistical limits dictated by the statistical distribution of the parameters involved. Full analysis of cable coupling must then include statistical analysis.

Calculating statistical parameters is very time consuming and often impossible. Solving complex systems using a Monte Carlo approach is not very feasible as it uses several hundred thousand simulations to obtain the statistics of the final result. Unscented Transforms UT offers a way of greatly reducing the computational burden needed during statistical analysis. In this work I have explored its application to cable coupling.

3.1 Statistical parameters

The property of cable coupling is quantified by a nonlinear function the parameters of which may have a random or statistical variation. The resulting cable coupling will then also have some form of probability distribution the nature of which needs to be quantified. The probability distribution defines the probability that a certain variable falls within a particular interval. There are many families of probability distributions such as normal distribution, binomial distribution, exponential distribution and uniform distribution. Each distribution function has a form which can be characterized by its mean, median, mode, variance skewness and kurtosis.

For a random variable x with a probability distribution $p(x)$ the mean or expected value of x is given by

$$E(x) = \int xp(x)dx \tag{69}$$

The median m of a probability distribution is defines as

$$\frac{1}{2} = \int_{-\infty}^{m} p(x)dx = \int_{m}^{\infty} p(x)dx \tag{70}$$

The mode of the distribution function is defined as point at which the distribution function takes its maximum value.

The variance σ^2 of a probability distribution gives a measure of the probable range of results and is defined by

$$\sigma^2 = \int (x-\mu)^2 p(x)dx \tag{71}$$

The skewness is a measure of the asymmetry or the probability distribution function and is given by

$$\gamma_1 = \frac{\int (x-\mu)^3 p(x) dx}{\sigma^3} \tag{72}$$

The measure of the peakedness of the probability function is given by its kurtosis which is defined as

$$\gamma_2 = \frac{\int (x-\mu)^3 p(x) dx}{\sigma^3} - 3 \tag{73}$$

In this work we we consider only normal and uniform distributions which are probably most representative of the distribution of the parameters involved. The normal distribution or Gaussian distribution of a variable x is given by

$$p(x) = \frac{1}{\sigma\sqrt{2\pi}} \exp\left(-\frac{(x-\mu)^2}{2\sigma^2}\right) \tag{74}$$

where μ is the mean, mode and median of the random variable, σ^2 is the variance of the random variable and the skewness and excess kurtosis of the distribution is zero.

A uniform distribution for the range a to b is defined as:

$$\begin{array}{ll} p(x) = \frac{1}{b-a} & a \leq x \leq b \\ p(x) = 0 & (x < a) \ \vee \ (x > b) \end{array} \tag{75}$$

The mean and median of this distribution is $(a+b)/2$, the variance is $(b-a)^2/12$, the skewness is zero and the kurtosis is $-6/5$.

3.2 The Unscented Transform (UT)

The description of UT reproduced here can also be found in [11] but is repeated here for completeness.

The UT was developed by Julier and Uhlman in 1997 [12] and it is similar to the Moment Design Technique (MDT) [13]. Both methods use the moments of the probability distribution function to develop the selection of points needed to solve for the probability distribution of the mapping function. In MDT, these points are called design values. In the UT approach they are the Sigma points S_i.

The main idea of the UT is to approximate the effect of an arbitrary nonlinear mapping by the mapping of the set of sigma points. Once the mapping is complete the statistical moments of the mapping are available form the weighted average of the mapped values at the sigma points.

3.2.1 Calculation of the sigma points

Let $G(\overline{U} + \widehat{u})$ be the continuous nonlinear mapping of a random variable $\widehat{u}$ of average value $\overline{U}$ and known probability distribution. The mapping can be

expressed by the Taylor polynomial expansion:

$$G(\overline{U}+\widehat{u}) = G(\overline{U}) + \frac{dG}{du}\widehat{u} + \frac{1}{2!}\frac{d^2G}{du^2}\widehat{u}^2 + \frac{1}{3!}\frac{d^3G}{du^3}\widehat{u}^3 + ... \tag{76}$$

This can then be written in the more compact form as

$$G(\overline{U}+\widehat{u}) = G(\overline{U}) + p(\widehat{u}) \tag{77}$$

The expected value of the nonlinear mapping is then

$$\overline{G} = E\{G(\overline{U}+\widehat{u})\} = E\{G(\overline{U})\} + E\{p(\widehat{u})\} = G(\overline{U}) + \overline{P} \tag{78}$$

In equation(78) $\overline{P}$ is the expected value of the Taylor polynomial. The variance of the nonlinear mapping is:

$$\sigma_g^2 = E\left\{[G(\overline{U}+\widehat{u}) - \overline{G}]^2\right\} = E\left\{p(\widehat{u})^2\right\} - \overline{P}^2 \tag{79}$$

This Taylor representation is also applicable to the sigma points.

$$G(\overline{U}+S_i) = G(\overline{U}) + p(S_i) \tag{80}$$

The polynomial is the same if the sigma points belong to the probability distribution of $\widehat{u}$. The comparison of the expected value and the variance of 80 with 78 and 79 results in the set of equations for the sigma points.

$$w_0 = 1 - \sum_i w_i \tag{81}$$

$$\sum w_i S_i^k = E\{\widehat{u}^k\} \tag{82}$$

The order of the approximation k depends on how the polynomial is truncated. Therefore, the truncation of the Taylor polynomial determines the number and value of the sigma points S_i as well as the weights w_i of the UT.

The set of equations for the sigma points 81 and 82 is nonlinear. Thus there are a number of possible choices for the sigma points satisfying the equation system. However, there is a set of solutions that are the roots to the polynomials of the Gaussian quadrature integration scheme [15]. This simplifies the solution of 81 and 82, since the weights and sigma points are more easily calculated from the Gaussian quadrature integration scheme. Naturally the interpolation polynomial is dependent on the probability distribution of $\widehat{u}$ (equivalent to the weighted function $w(\widehat{u})$ of the integration). Table I presents the normalized sigma points and weights for the two probability distribution systems considered. The normalization factor is the standard deviation in the Gaussian distribution case. For the uniform distribution, the normalized factor is the interval of the distribution [-1,1].

Table I UT Sigma points and weights

	Normalized sigma points and weights		
Order	**Weights**	**Sigma Points**	**Probability Distribution**
1	0.5 0.5	-0.577 0.577	$w(\widehat{u}) = \frac{1}{2} \quad \lvert\widehat{u}\rvert < 1$ $w(\widehat{u}) = 0 \quad \lvert\widehat{u}\rvert > 1$
2	0.278 0.444 0.278	-0.775 0 0.775	
4	0.119 0.239 0.284 0.239 0.119	-0.906 -0.538 0 0.538 0.906	
1	0.5 0.5	-1 1	$w(\widehat{u}) = \frac{1}{\sigma\sqrt{2\pi}} \exp\left(-\frac{\widehat{u}^2}{2}\right)$
2	0.167 0.666 0.167	-1.73 0 1.73	
4	0.011 0.222 0.534 0.222 0.011	-2.857 -1.356 0 1.356 2.857	

3.2.2 Calculation of the moments of the mapped distribution

Once the sigma points are known, it is straightforward to apply them to the nonlinear mapping. The statistical moments are calculated using:

$$E\left\{G(\overline{U}+\widehat{u})^n\right\} = \sum_i w_i G(\overline{U}+S_i)^n \tag{83}$$

The central moments are calculated using the expected value of the mapping (83 with n =1). The general expression is

$$E\left\{\left[G(\overline{U}+\widehat{u})\right]^n\right\} = \sum iw_i\left[G(\overline{U}+S_i)-\overline{G}\right]^n \tag{84}$$

The calculation of the resulting statistical moments is linked to the form of the nonlinear function. If the nonlinear function is expressed in an analytical form then the demoralized sigma points are used in the calculation. For example consider the calculation of the first resonant frequency of a dielectric filled cavity where the permittivity is a random variable. The nonlinear mapping function has the form:

$$G(\varepsilon_r+\widehat{u}) = \frac{f_0}{\sqrt{\varepsilon_r+\widehat{u}}} \tag{85}$$

where f_0 is the resonant frequency for a cavity filled with free space, ε_r is the mean value of the permittivity and $\widehat{u}$ is a zero mean random variable. The distribution of the random variable determines the weights and sigma points. As discussed in the previous section, the denormalization factor depends on the type of distribution. For the uniform distribution, the variable will be demoralized by the size of the interval. In the case of the normal distribution, the denormalization factor is the standard deviation. The nonlinear function 85 is calculated for each sigma point and the moments are obtained using 83 and 84.

If the nonlinear function is numerical, such as resulting from a numerical simulation, then the process has to be repeated for each sigma point.

3.2.3 Accuracy of the unscented transform

The accuracy of the UT is dependent on the order of the approximation as presented in Table I. If the sigma points are obtained from the quadrature scheme, then the accuracy will be the same as the chosen interpolation polynomial. As an example one can compare the expected value and central moments if an exact calculation is possible. This is the case of the nonlinear mapping given by 85. In this example let $f_0 = 300$ MHz, $\varepsilon_r = 4$ and $3 < \widehat{u} < 5$. Thus for the uniform distribution the interval is [4-1, 4+1] and for the Gaussian distribution this results in a standard deviation of 1/3 (considering a 99% confidence interval). The sigma points, weights and results for 2nd order accuracy are then:

Uniform distribution

$$G(4 - 0.775) = \frac{300}{\sqrt{4-0.775}} = 167.054$$

$$G(4) = \frac{300}{\sqrt{4}} = 150$$

$$G(4 + 0.775) = \frac{300}{\sqrt{4+0.775}} = 137.289$$

Thus the expected value from 83 is $0.278 \times 167.054 + 0.444 \times 150 + 0.278 \times 137.289 = 151.206$ MHz.

Normal distribution

$$G(4 - \tfrac{1.73}{3}) = \frac{300}{\sqrt{4-0.577}} = 162.142$$

$$G(4) = \frac{300}{\sqrt{4}} = 150$$

$$G(4 + \tfrac{1.73}{3}) = \frac{300}{\sqrt{4+0.577}} = 140.231$$

Thus the expected value from 83 is $0.167 \times 167.054 + 0.666 \times 150 + 0.167 \times 137.289 = 150.398$ MHz.

Table II shows the comparison of the UT calculations with exact analytical results. In this table, the moments are calculated using 2, 3, and 5 sigma points (As listed in Table I).

Table II UT Comparison with Exact Results

Type of moment	**Type of distribution**			
	Uniform (UT)	**Uniform (Exact)**	**Normal (UT)**	**Normal (Exact)**
Expected Value (MHz)	151.189	151.205	150.363	150.397
	151.206		150.398	
	151.205		150.4	
Standard Deviation (MHz)	10.962	11.143	6.277	6.36
	11.143		6.364	
	11.144		6.36	
skewness	0	0.266	0	0.39
	0.266		0.388	
kurtosis	-2	-1.109	-2	0.322
	-1.19		0.04	
	-1.109		0.32	

The results indicated in Table II shows how the order of accuracy is related to the number of sigma points. It also shows that for nonlinear mappings the resulting probability distribution is different from that of the variable although it is dependent on it.

3.2.4 The multivariate Unscented Transform

The multiple random variable case can also be modelled by the UT. It is possible to include either independent or correlated variables. Although the approach allows for correlated variables, it is best to calculate the sigma points for independent random variables. Once these points are known, they can be processed by a linear transformation using the covariance matrix.

In multivariate cases, the choice of sigma points and weights is not unique and it is usually necessary to use additional sigma points [16]. There are many possible sets that may be used. One set that is simple to calculate is the combination of sigma points provided by the appropriate quadrature scheme. In this set, the weights are calculated by the product of individual weights of each random variable.

In most multivariate problems, some random variables may have a more dominant effect. This may be ascertained by careful analysis of the moments of the marginal distributions or by the analysis of the correlation of the input and output variables.

3.2.5 Estimation of a variables influence in the multivariate case

A numerical problem with several random variables may be well characterized by a smaller subset of variables if they are more dominant. Using the concept of marginal distribution probability function [16], it is possible to determine what are the most important variables. These distributions are essentially one-variable distributions, where the calculation is performed for each variable separately using 84. The resulting expected value and variance provides information

on the significance of each of the variables. Since the UT is based on the Taylor approximation of the nonlinear mapping , the calculation of the marginal statistical moments provides a good estimate of the influence of each parameter in the output result. For n variables the marginal statistical moments for the m variable can be found using:

$$I_{x_m} = \frac{E\left\{G(\overline{U_m})^2\right\} - E\left\{G(\overline{U_m})\right\}^2}{E\left\{G(\overline{U_1}, \ldots, \overline{U_n})^2\right\} - E\left\{G(\overline{U_1}, \ldots, \overline{U_n})\right\}^2} \tag{86}$$

where I_{xm} is the relative influence of variable $\overline{U_m}$ in the variance of the result.

4 Results

In this section the models for cable transfer impedance are compared with known behavior and measurements. From this it is deduced that the Kley model appears to give the most accurate results. Using the Kley model for the cable transfer impedance the cable coupling is then predicted for a range of cabling arrangements as investigated by two intern students [17] and [18].

4.1 Comparison of the transfer impedance models

4.1.1 Single braided cables

The predicted transfer impedance as given by the Vance, Tyne and Kley models for the common single braid cable type RG58 with the parameters as supplied by the manufacturers (RG58-Man in appendix) are given in Figure 7 . There are significant differences between the models but the models are all comparable to the typical results shown in Figure 8 [6] and a previous report [7] found that the Kley model gave the best results. Benson et al. [8] also reported that the Tyni model tended to over estimate the cable transfer impedance. Figure 9 shows the predicted transfer impedance using other RG58 parameters as given in [5] and by comparing this to Figure 7 this indicates by how much the transfer impedance may vary between manufacturers. In this report the Kley model and the parameters (RG58-Man) given in the appendix will be predominantly used for single braided cable.

Figures 10 - 12 show the predicted transfer impedances and their variance after applying a reasonable estimate of the manufacturers tolerances using the (RG58-Man) parameters. The assumed manufacturers tolerances are given in Table III are as used by Benson et al. [8] and the statistical distribution was assumed to be normal. Note that α and b are dependent variables.

Table III. Variance in braid parameters

σ_{D0}	σ_d	σ_l
0.13 mm	0.003 mm	1.979 mm

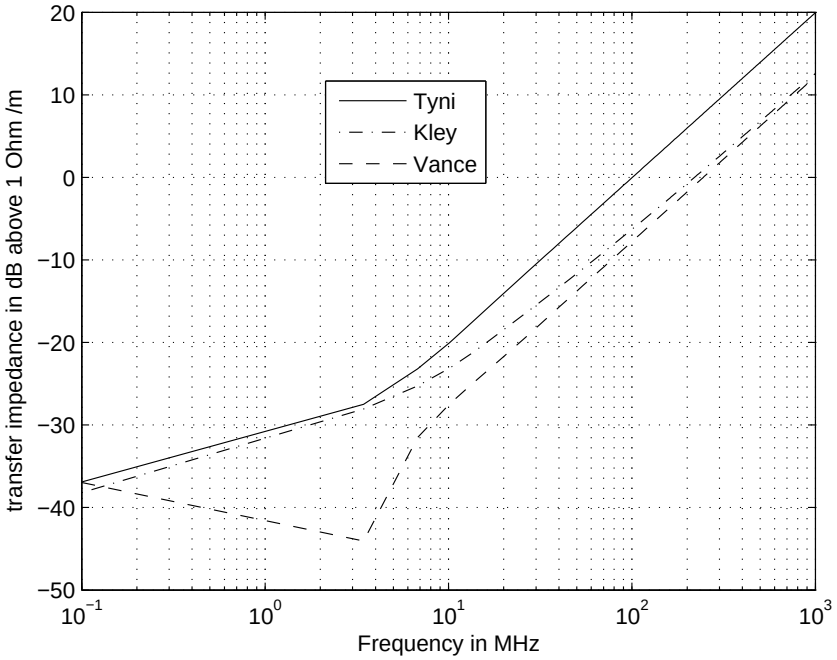

Figure 7: Predicted transfer impedance using parameters (RG58-Man.)

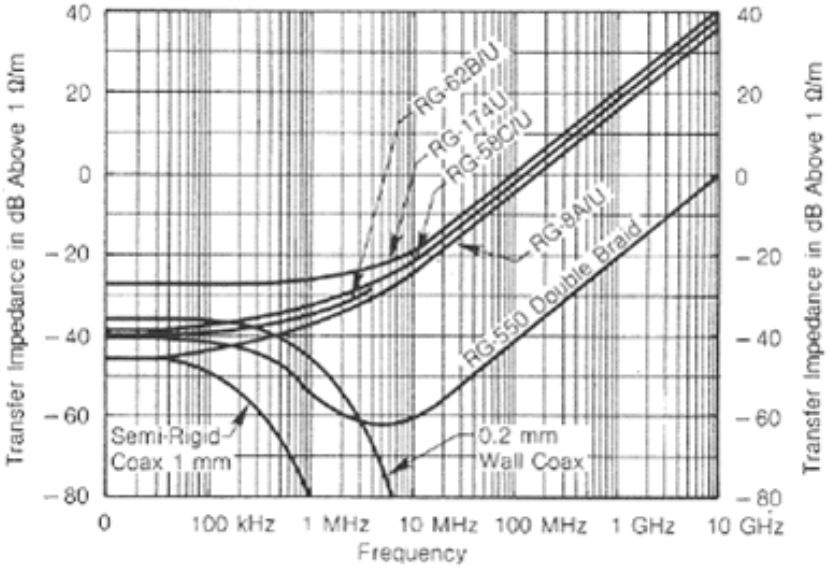

Figure 8: Typical transfer impedances of different cables [6]

The standard deviation, skew and kurtosis of the distribution of the predicted transfer impedances assuming a normal distribution for the tolerances are given in Figures 13 to 15. There is only a small skew and kurtosis so the variation in transfer impedance can be considered to be also a normal distribution.

4.1.2 Double braided cables

The double braided cable considered was the RG214 cable the parameters of which are given by Vance [5] and listed in the appendix. The predicted transfer impedance as given by 31 and using the Vance, Tyne and Kley models for the inner and outer braid transfer impedances are given in Figures 16 and 17 . There are significant differences between the models. The Kley model seems comparable to the typical results shown in Figures 18 and 19 from [19] and [20] although it seems to predict a small peak in the transfer impedance at around 100 kHz. In this report the Kley model for the inner and outer cable braids for the double braided cable and the parameters (RG214) given in the appendix will be predominantly used for single braided cable.

Figures 20 and 21 show the predicted transfer impedances and their variance after applying a reasonable estimate of the manufacturers tolerances using the (RG214) parameters. The assumed manufacturers tolerances are given in Table IV are consistent with that used by Benson et al. [8] and the statistical

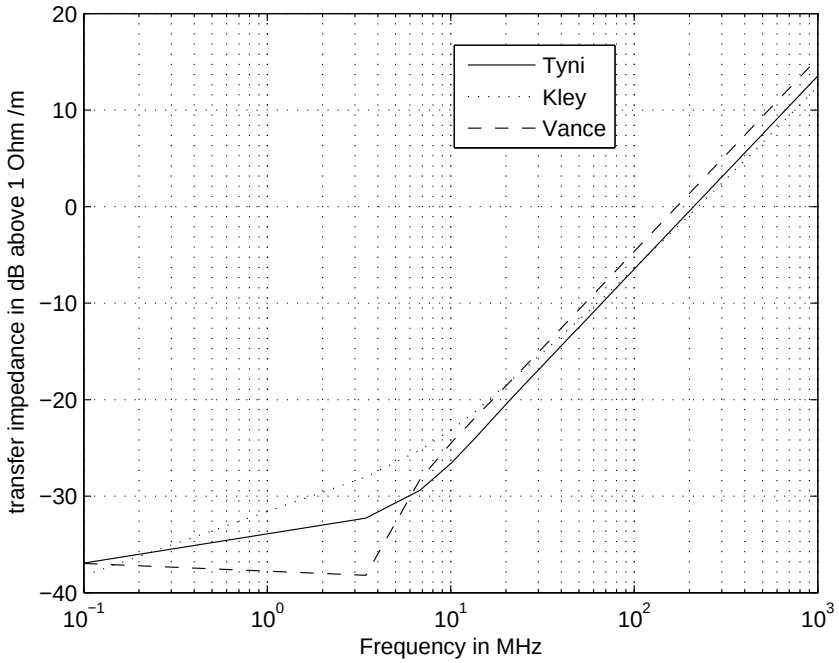

Figure 9: Predicted transfer impedance using parameters (RG58) [6]

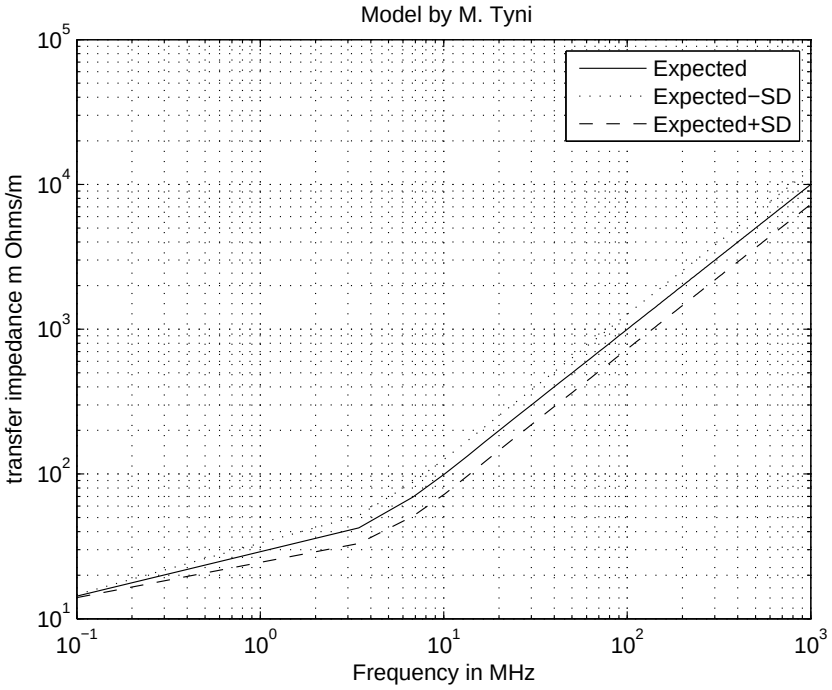

Figure 10: Predicted transfer impedance and its variance using the Tyni model [2] and manufacturing tolerances for (RG58-Man.)

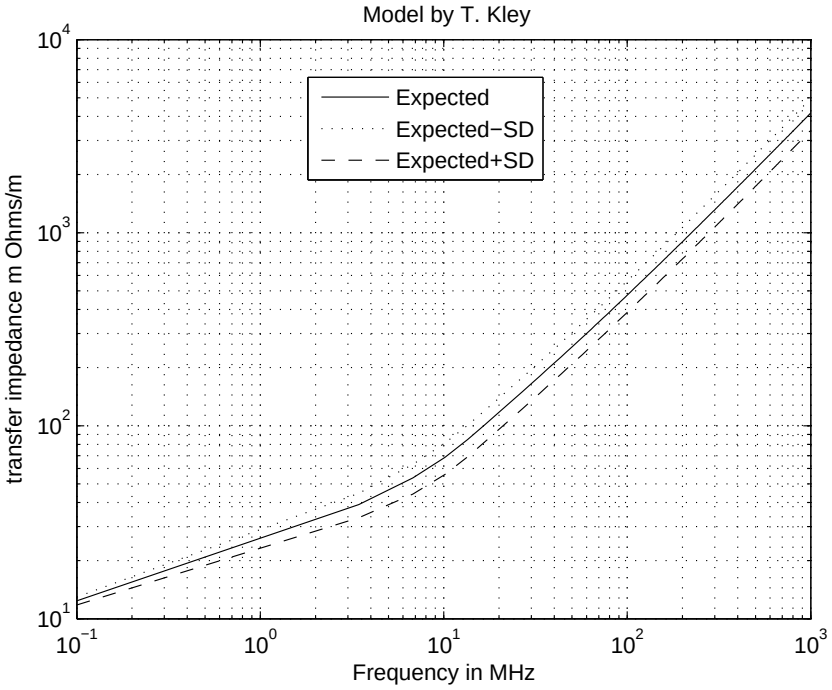

Figure 11: Predicted transfer impedance and its variance using the Kley model [3] and manufacturing tolerances for (RG58-Man.)

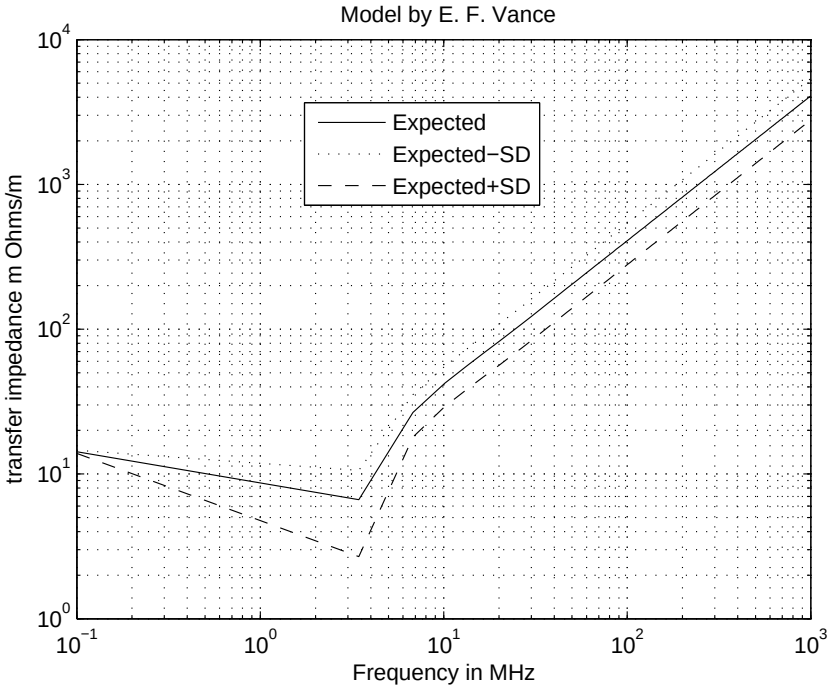

Figure 12: Predicted transfer impedance and its variance using the Vance model [1] and manufacturing tolerances for (RG58-Man.)

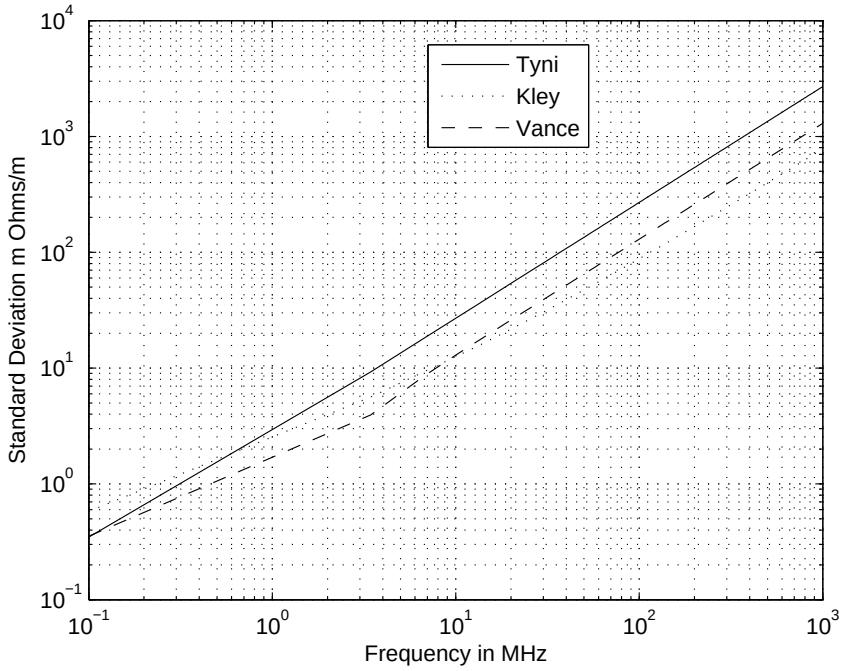

Figure 13: Predicted standard deviation in the transfer impedance using manufacturing tolerances for (RG58-Man.)

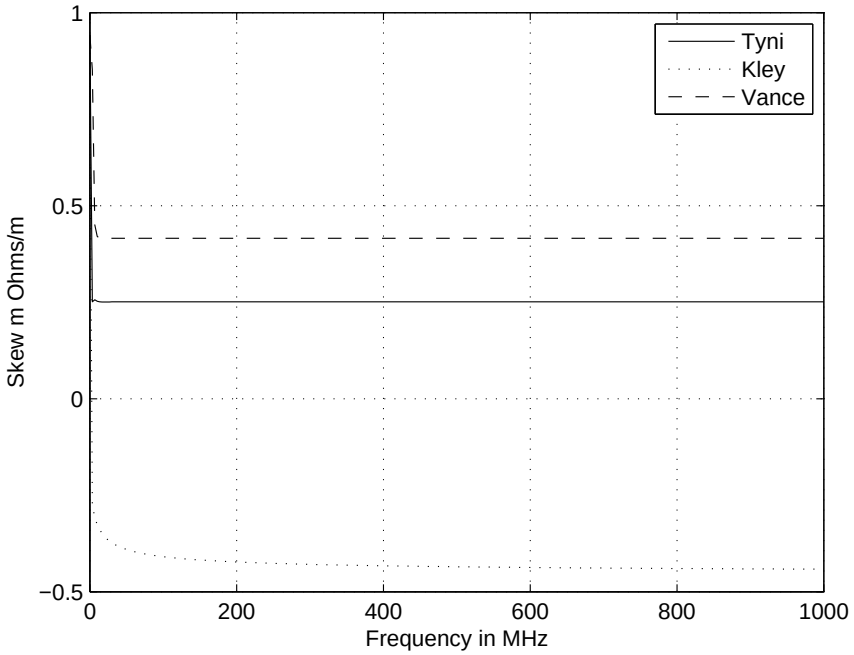

Figure 14: Predicted skew in the statistical distribution in the transfer impedance using manufacturing tolerances for (RG58-Man.)

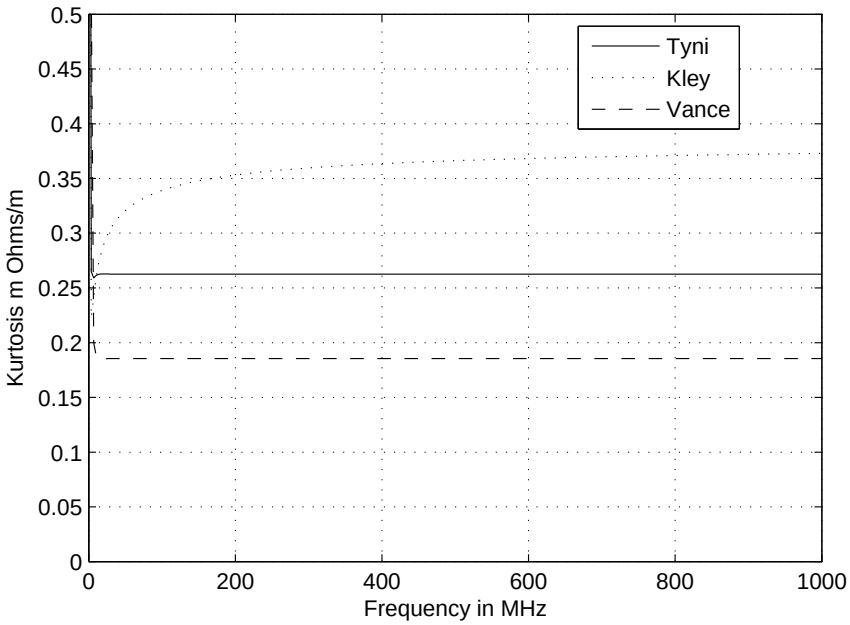

Figure 15: Predicted kurtosis in the statistical distribution in the transfer impedance using manufacturing tolerances for (RG58-Man.)

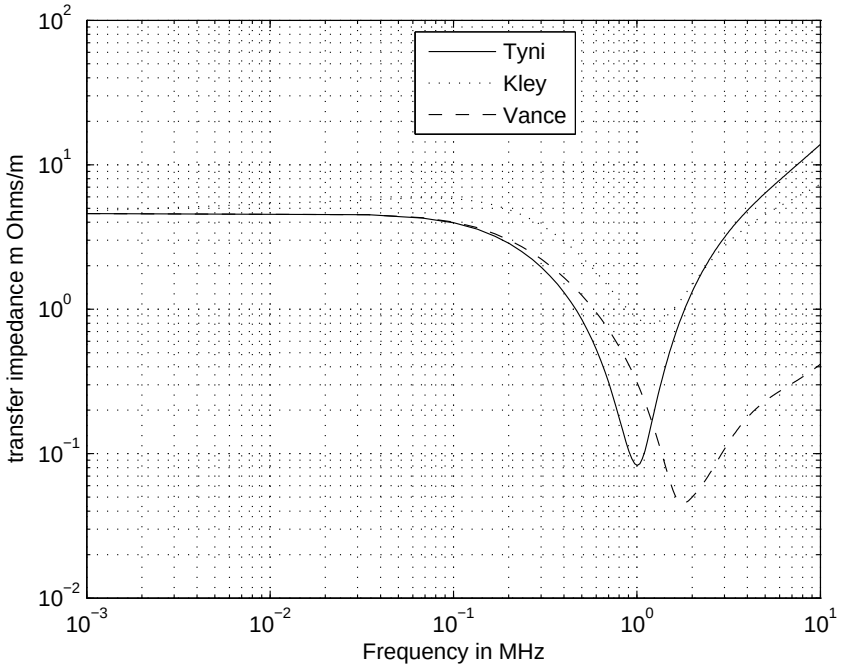

Figure 16: Predicted transfer impedance of a double braided cable using parameters (RG214)

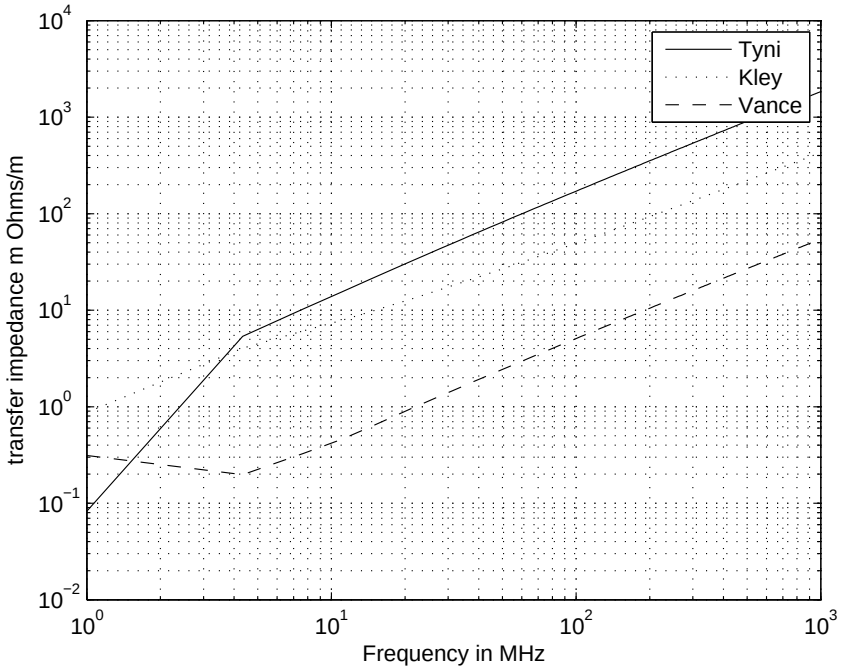

Figure 17: Predicted transfer impedance of a double braided cable using parameters (RG214.)

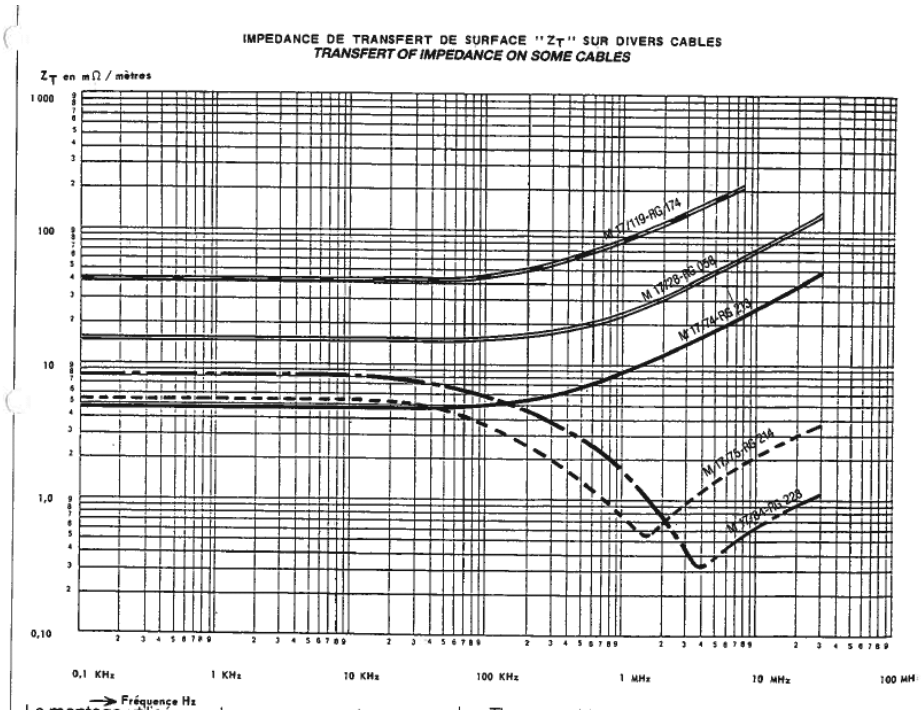

Figure 18: Data for transfer impedance of a double braided cable (RG214) from [19]

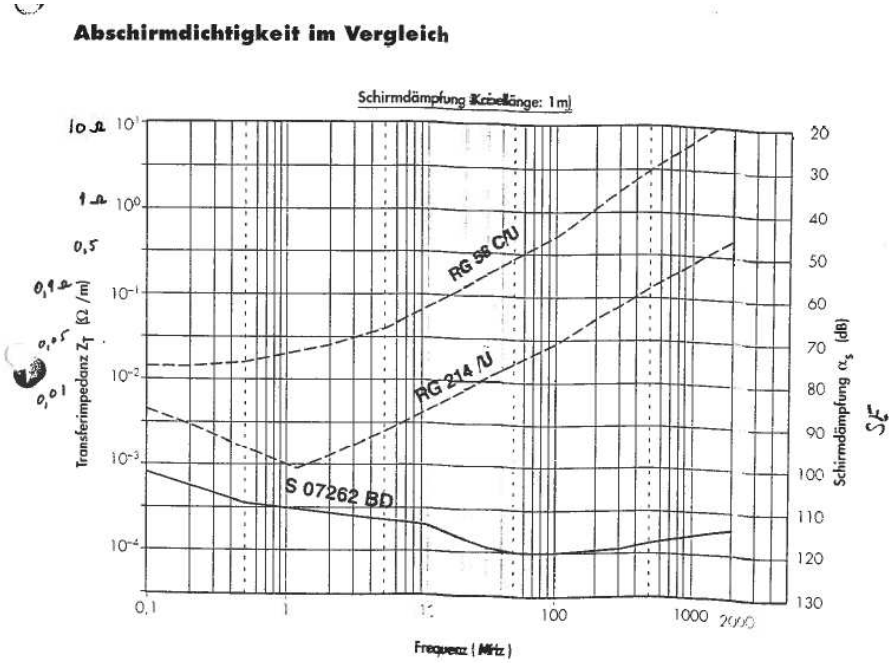

Figure 19: Data for transfer impedance of a double braided cable (RG214) from [20]

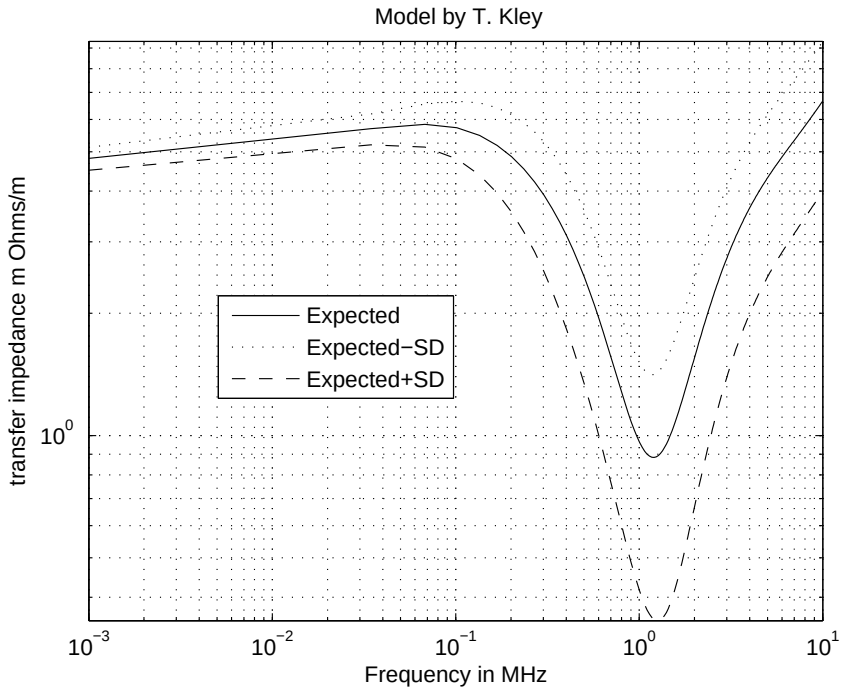

Figure 20: Predicted transfer impedance and its variance using the Kley model [3] and manufacturing tolerances for double braided cable(RG214)

distribution was assumed to be normal.

Table IV. Variance in double braid parameters

	σ_{D0}	σ_d	σ_l
Inner	0.37 mm	0.004 mm	1.836 mm
Outer	0.4 mm	0.004 mm	1.979 mm

4.2 Predicted and measured cable coupling

For this study results were used from the internship reports by Leon Korteweg [17] and Tom Wijnands [18]. The reports contain an extensive set of measurements but there was only time to study some results from cable to cable coupling of RG58 coaxial cables and wire to cable coupling of double braided RG214 coaxial cables.

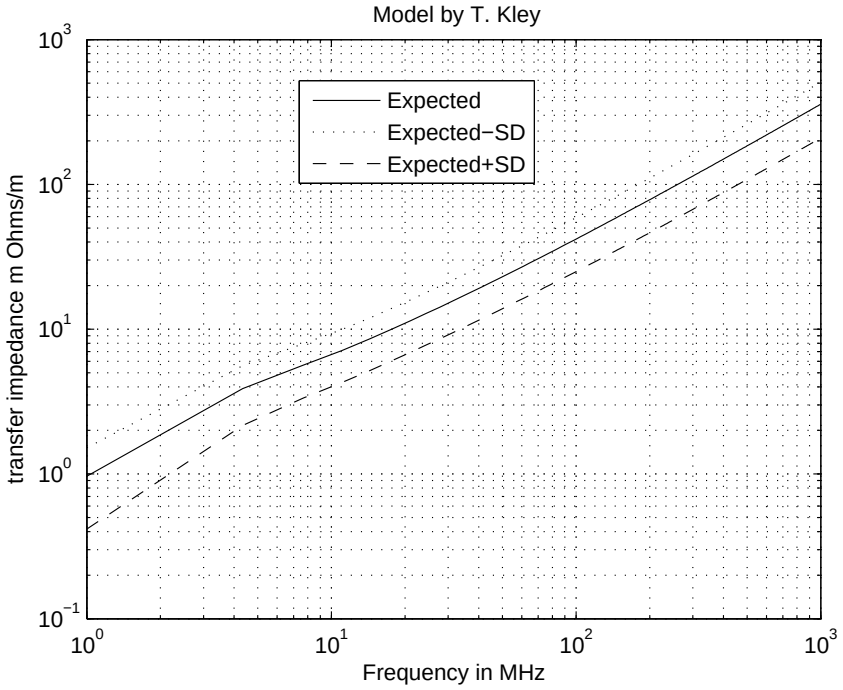

Figure 21: Predicted transfer impedance and its variance using the Kley model [3] and manufacturing tolerances for double braided cable(RG214)

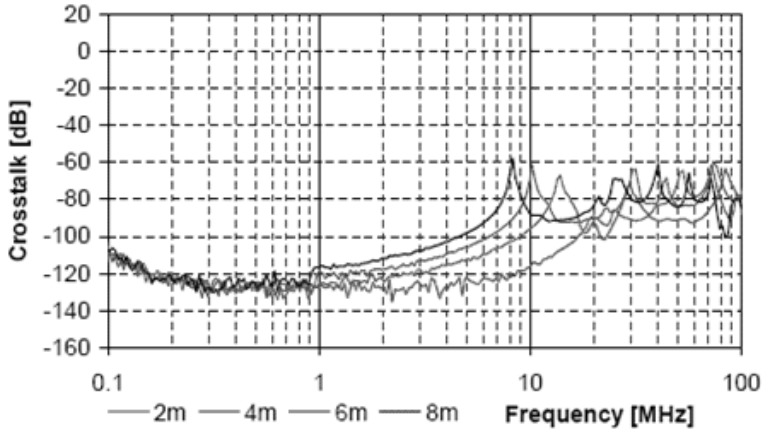

Figure 22: Measurement of Crosstalk at different cable lengths (2× RG58, d=5cm, for floating cables) [17].

4.2.1 Single braided cable (RG58)

In the first example using single braided cable three different configurations were considered. The first configuration was of cables which had electrically isolated terminations and were nor located near to a conducting earth ground plane. These cables were called floating cables and a range of cable lengths were investigated. A typical set of results for this configuration are given in Figure 22 from [17]. Note that no comparable set of results were found from [18] report.

In the second example the cables were 2m long and they terminated into the same connector plate so the termination earths were electrically connected. There was no conducting ground plane for this example. Typical results for this configuration are given in Figure 23from [18] respectively.

In the third and final example the cables were also 2m long and terminated into the same connector plate so the termination earths were electrically connected. But there was a conducting ground plane for this example that was also electrically connected to the terminating end plates. Typical results for this configuration are given in Figure 24from [18] respectively.

What is immediately apparent in the results provided from [17] and [18] is that the first resonance does not correspond to the expected half wavelength frequency (75MHz for a cable length of 2m) therefore stray reactances in the tertiary circuit must be important (the victim and source cable circuits have matched loads so do not resonate).

The simulation of the "floating" cables using a tertiary circuit termination impedance of 10 pF to represent stray capacitance and using the high frequency model is shown in Figure 25. The model appears to predict the resonances

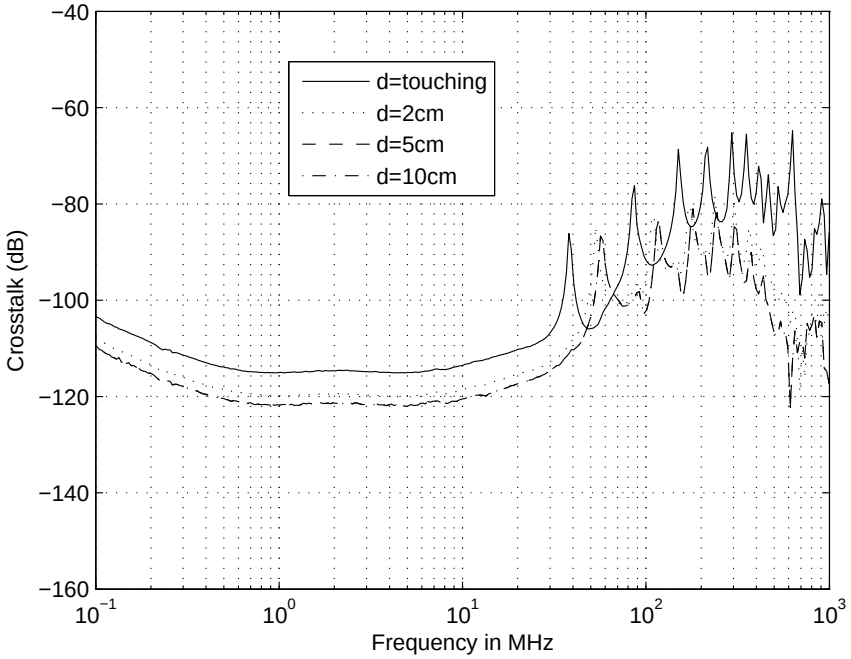

Figure 23: Measurement of Crosstalk in two RG58 coax cables (l= 2m, and common connector plates) [18].

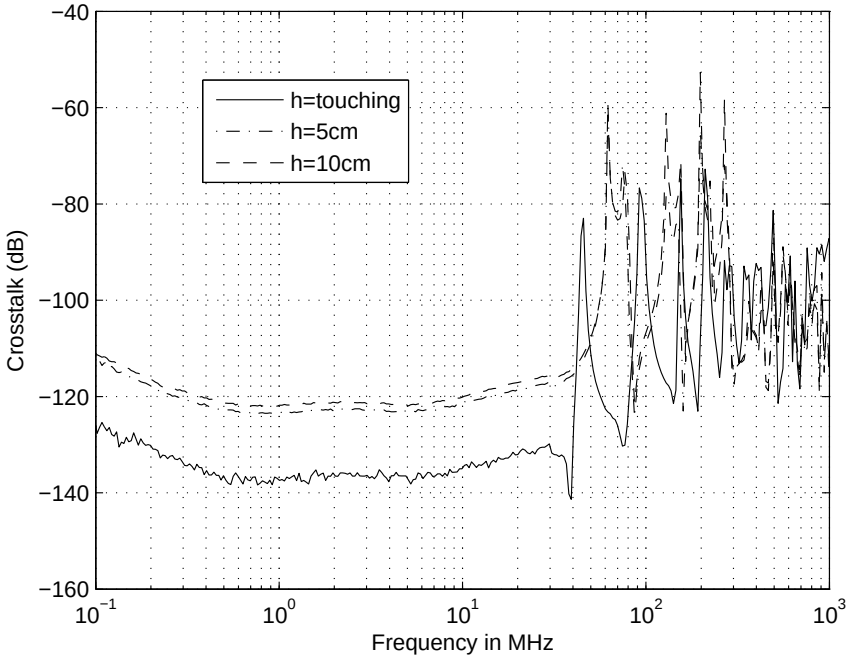

Figure 24: Measurement of Crosstalk in two RG58 coax cables (l= 2m, common connector plates and ground conducting tray, d= 2cm) [18].

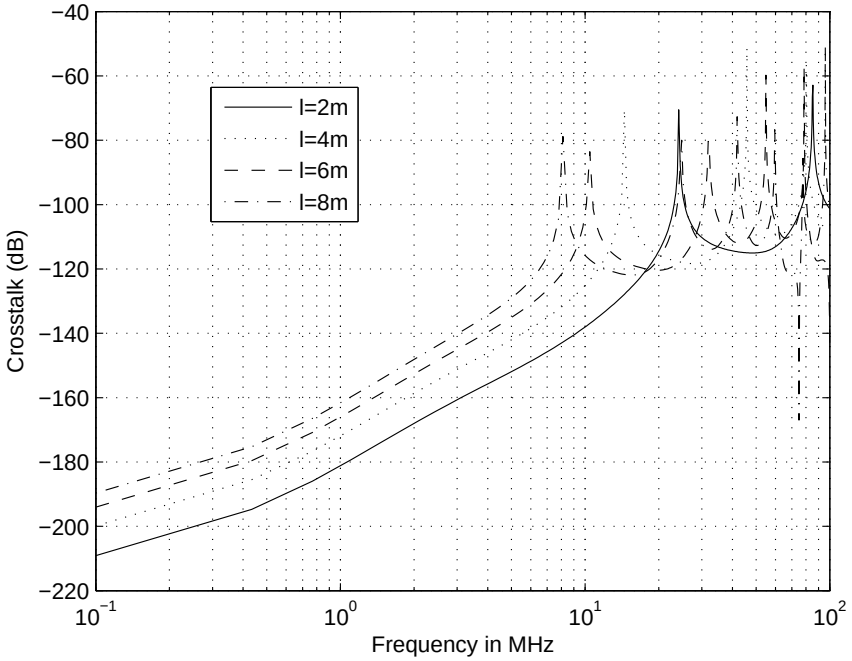

Figure 25: Simulation Crosstalk in two RG58 coax cables (d= 5cm, and **no** common connector plate at remote termination) using a high frequency model and the Kley model [3]of the transfer impedance

reasonably well. But the overall the coupling appears to be about 20 dBs too low and this may possibly due to manufacturing tolerances of the braid or incorrect braid data. Below 1 MHz the observed cable coupling is a lot greater than the predicted coupling but this may be due to the noise floor of the measurements.

The theoretical prediction for the coupling between the 2m length cables with the common connector plates and no ground plane using the low frequency model is given in Figure 26. Notice that this model can not predict the point at which there is resonance in the tertiary circuit leading to an increased cable coupling.

Figure 27 shows the simulation results for the more complete high frequency model and giving the tertiary terminations as a stray inductance of 0.4 μH to represent the loop inductance at the connector plate. The results in Figure 27 compare reasonably well with the measurements. The resonant frequencies of the peaks are the same, but this depends on the approximated tertiary terminal impedance. To aid direct comparison the measurements and simulations are combined in Figures 28 and 29. The overall predicted coupling is about 10 dBs lower than the measurements. This may be due to the model of the cable transfer

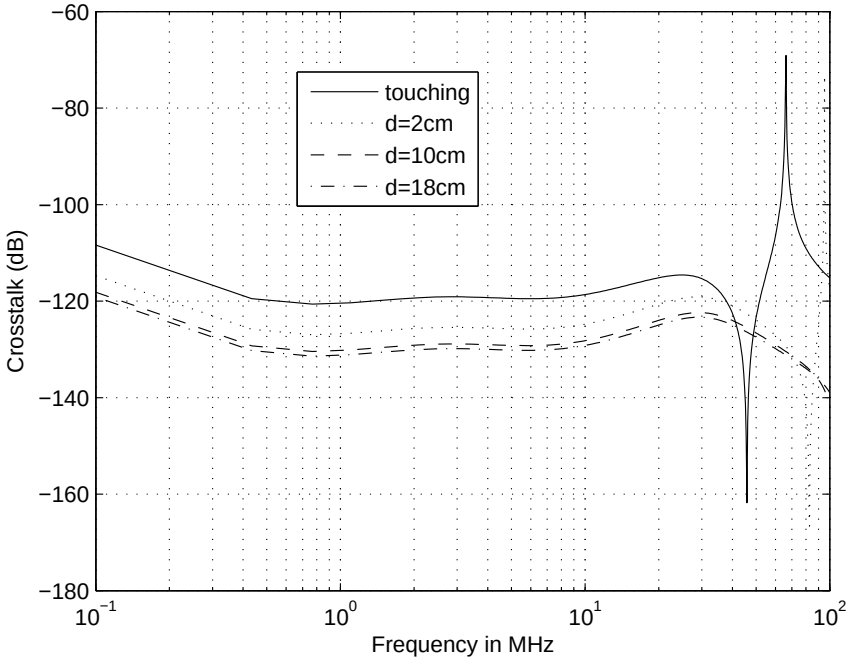

Figure 26: Simulation Crosstalk in two RG58 coax cables (l= 2m, and common connector plates) using a simple low frequency model and the Kley model of the transfer impedance.

impedance. Figure 30 Shows the predicted cable crosstalk using the upper bound of the expected transfer impedance given the manufacturing tolerances of the cable braid. This result agrees better with the measurement results and it can also be noticed that errors in the predicted transfer impedance does not affect the predicted resonant frequencies. The other possibility is that the Kley model [3]is not sufficiently accurate. Simulations using the Vance [1] and Tyni [2] transfer impedance models are given in Figures 31 and 32 respectively. It appears that the Tyni and Vance models do not reproduce the observed cable cross coupling as well as the Kley model.

The theoretical prediction for the coupling between the 2m length cables with the common connector plates with a connecting ground plane using the complete high frequency model and giving the tertiary terminations as a stray common mode inductance of 0.125 μH and differential mode inductance of 0.135 μH to represent the termination inductance at the connector plate is given in Figure 33. The results in Figure 33 compare reasonably well with the measurements. The resonant frequencies of the peaks are the same, but this depends on the approximated tertiary terminal impedance. To aid direct comparison the mea-

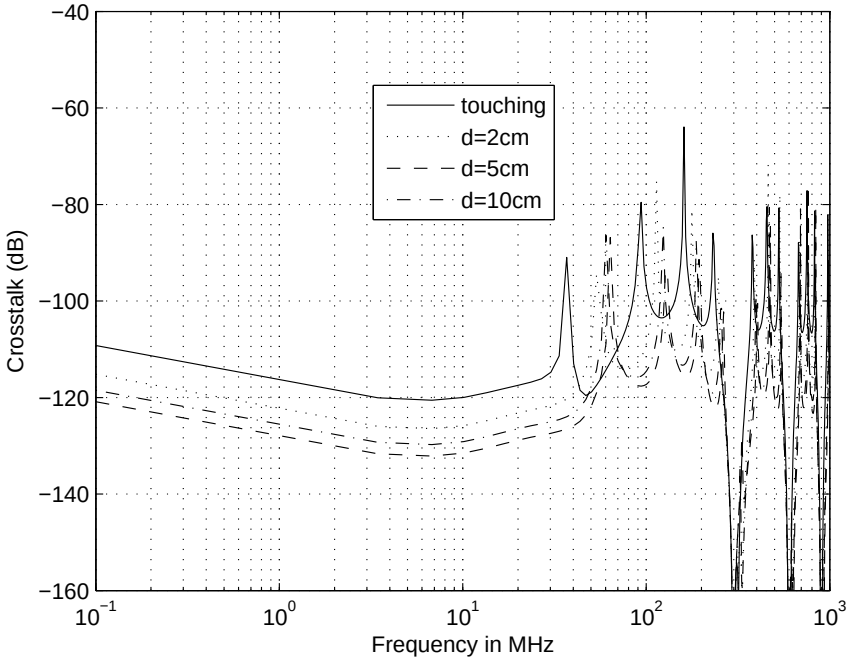

Figure 27: Simulation Crosstalk in two RG58 coax cables (l= 2m, and common connector plates) using a high frequency model and the Kley model [3] of the transfer impedance.

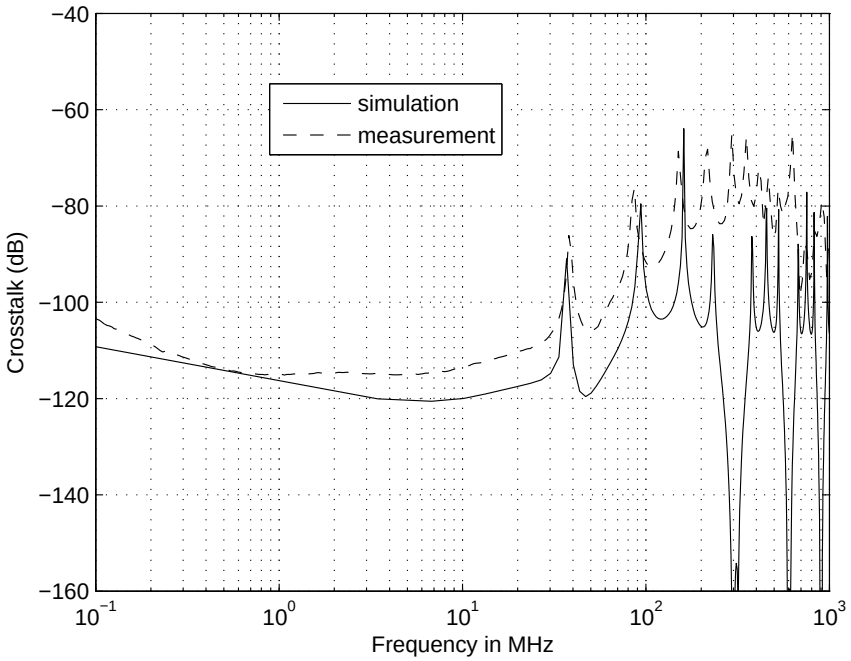

Figure 28: Simulation Crosstalk in two RG58 coax cables compared with measurement (l= 2m, and common connector plates, d=touching) using a high frequency model and the Kley model [3] of the transfer impedance.

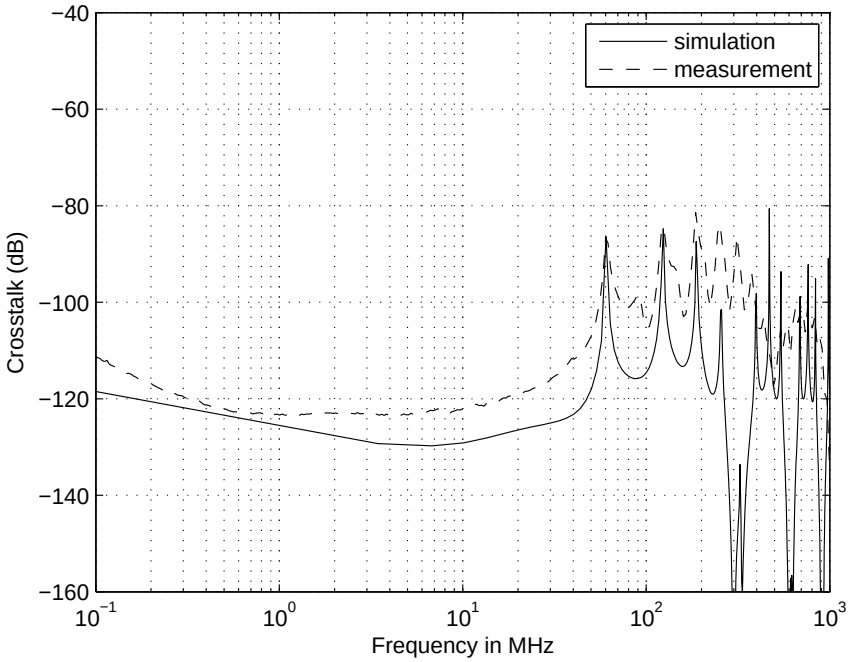

Figure 29: Simulation Crosstalk in two RG58 coax cables compared with measurement (l= 2m, and common connector plates, d=10cm) using a high frequency model and the Kley model [3] of the transfer impedance.

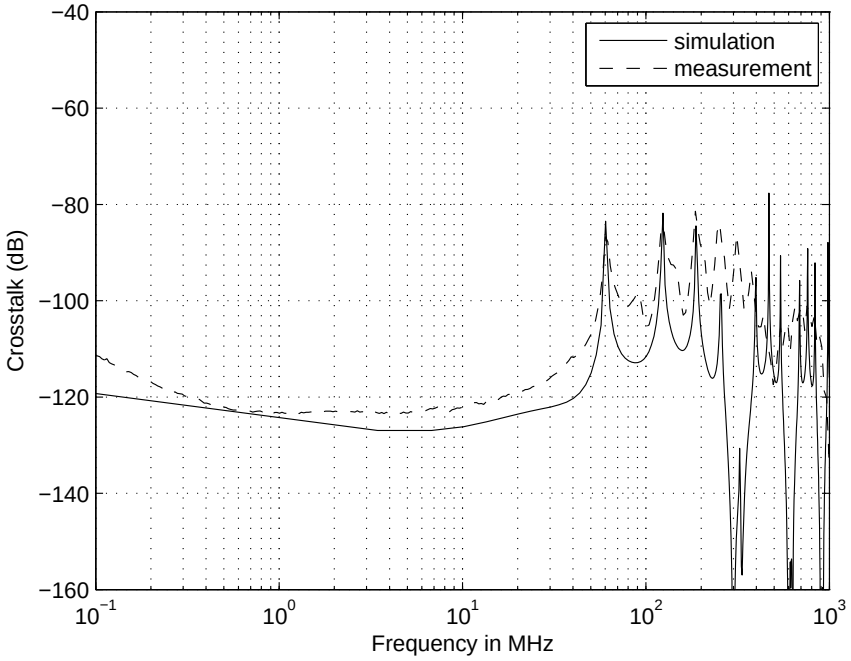

Figure 30: Simulation Crosstalk in two RG58 coax cables compared with measurement (l= 2m, and common connector plates, d=10cm)using a high frequency model and the Kley model [3] of the transfer impedance and the upper bound of the expected transfer impedance ($Z_t + \sigma_{Zt}$) given manufacturing tolerances.

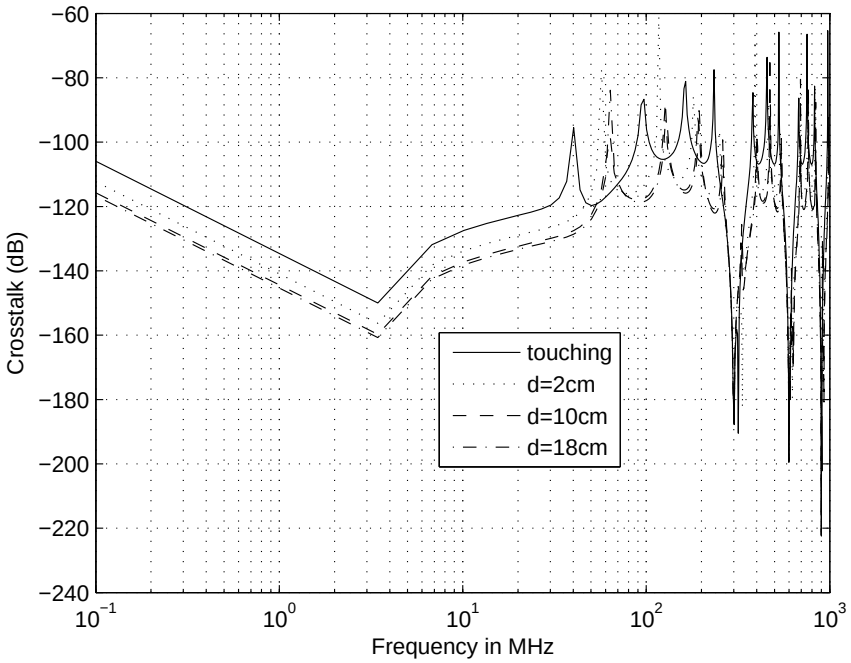

Figure 31: Simulation Crosstalk in two RG58 coax cables (l= 2m, and common connector plates) using a high frequency model and the Vance model [1] of the transfer impedance

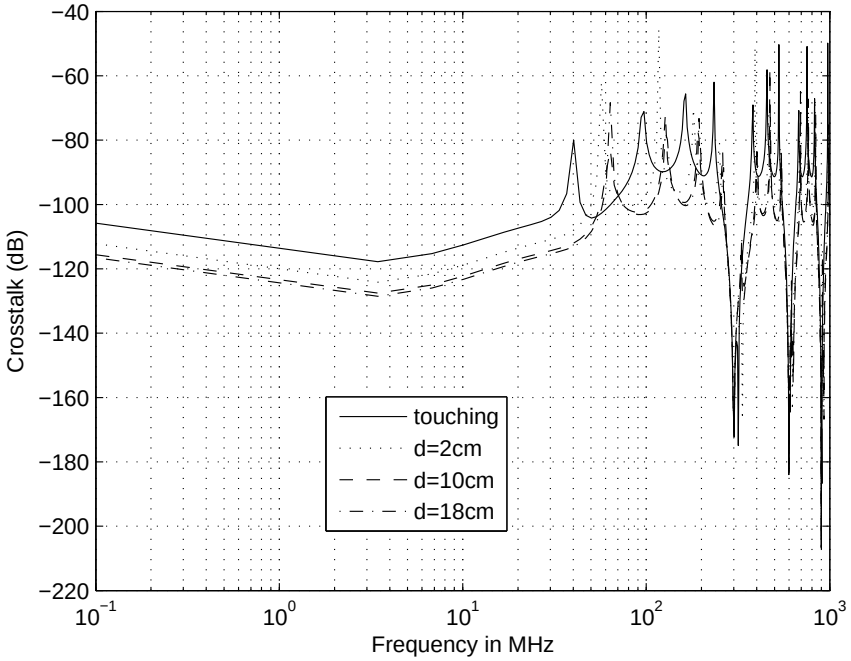

Figure 32: Simulation Crosstalk in two RG58 coax cables (l= 2m, and common connector plates) using a high frequency model and the Tyni model [2]of the transfer impedance

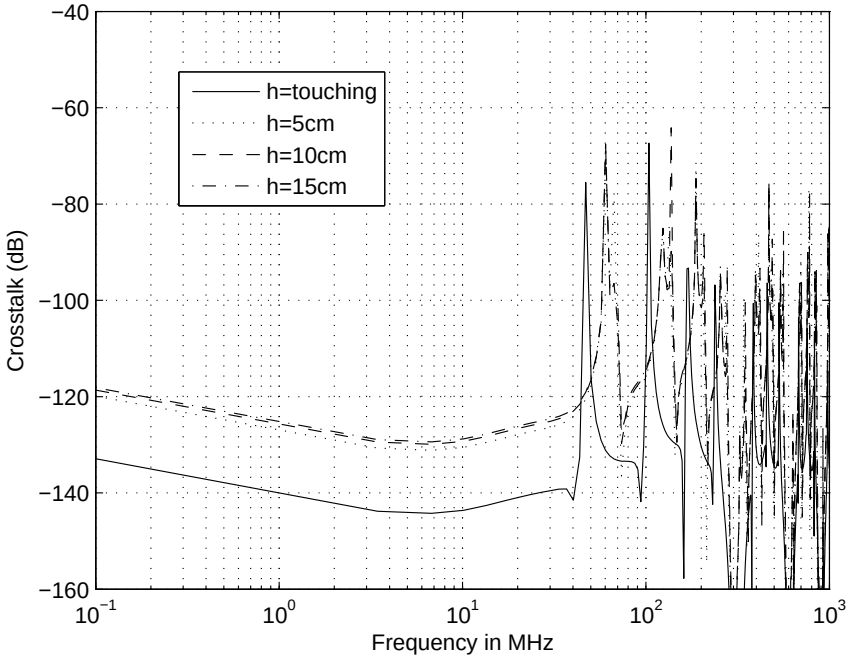

Figure 33: Simulation Crosstalk in two RG58 coax cables (l= 2m, and common connector plates and ground plane) using a high frequency model and the Kley model [3] of the transfer impedance.

surements and simulations are combined in Figures 34 and 35. The overall predicted coupling is again about 10 dBs lower than the measurements.

4.2.2 Double braided cable (RG214)

In the second example using double braided cable because of the low transfer impedance the victim cable was excited by a parallel wire. To demonstrate double braided cable only one example configuration was considered necessary and that was the wire and cable attached to a common connector plate with a common conducting ground plane. Typical results for this configuration are given in Figures 36 from [18].

The theoretical prediction for the coupling between a 2m length wire and a 2m coaxial double braided cable with the common connector plates with a connecting ground plane using the complete high frequency model and giving the tertiary terminations as a stray common mode inductance of 0.125 μH and differential mode inductance of 0.135 μH to represent the termination inductance at the connector plate is given in Figure 37. The results in Figure 37

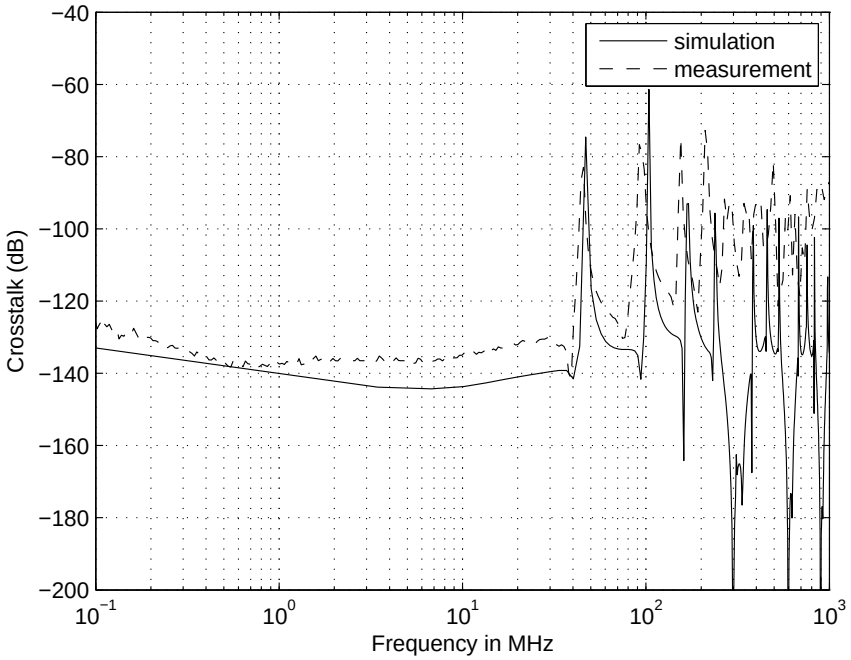

Figure 34: Simulation Crosstalk in two RG58 coax cables compared with measurement (l= 2m, and common connector plates and ground plane, height=touching) using a high frequency model and the Kley model [3] of the transfer impedance.

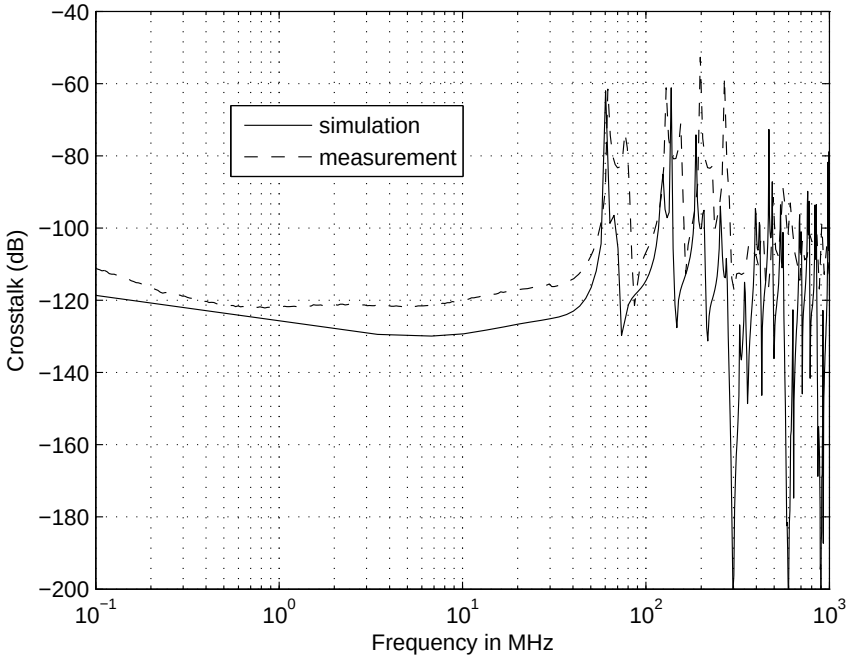

Figure 35: Simulation Crosstalk in two RG58 coax cables compared with measurement (l= 2m, and common connector plates, height=10cm) using a high frequency model and the Kley model [3] of the transfer impedance.

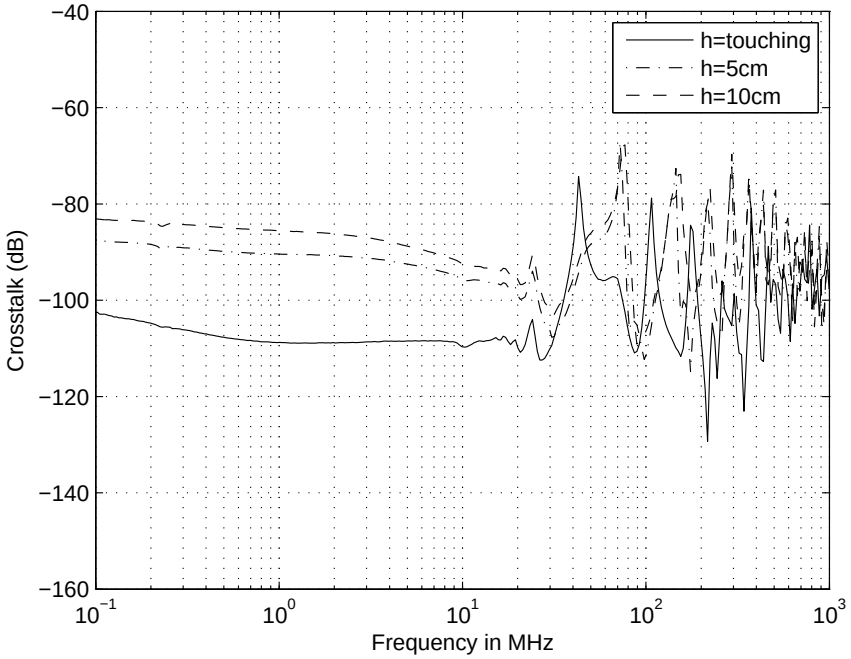

Figure 36: Measurement of Crosstalk between a wire and a RG214 coax cable (l= 2m, common connector plates and ground conducting tray, d= 5cm) [18].

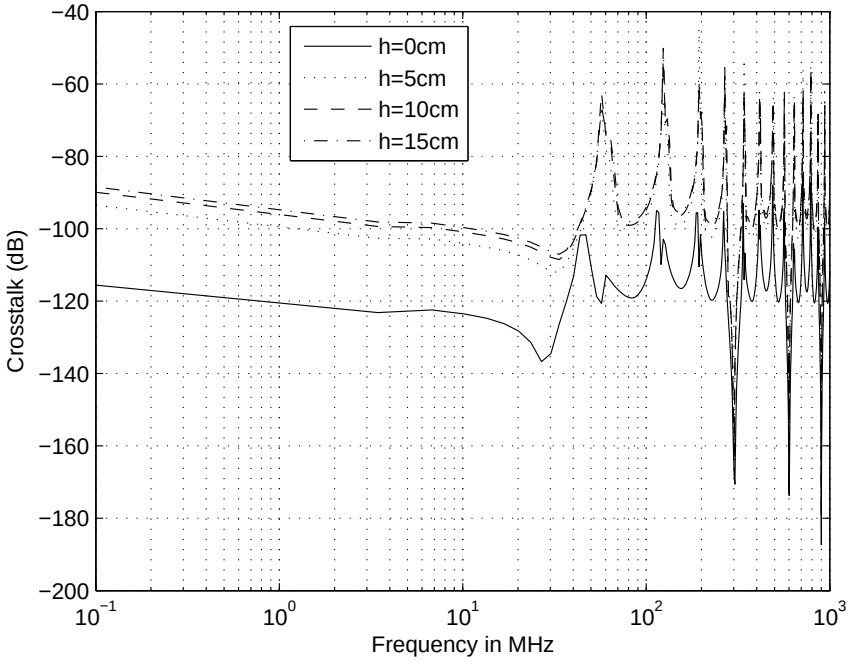

Figure 37: Simulation Crosstalk between a wire and RG214 coax cable (l= 2m, and common connector plates and ground plane) using a high frequency model and the Kley model [3] of the transfer impedance.

compare reasonably well with the measurements. The resonant frequencies of the peaks are the same, but this depends on the approximated tertiary terminal impedance. To aid direct comparison the measurements and simulations are combined in Figures 38 and 39. The overall predicted coupling is again about 10 dBs to 10 dBs lower than the measurements. Figure 40 Shows the predicted cable crosstalk using the upper bound of the expected transfer impedance given the manufacturing tolerances of the cable braid. This result agrees only slightly better with the measurement results and it can also be noticed that errors in the predicted transfer impedance does not affect the predicted resonant frequencies.

4.3 Prediction of the peak cable coupling

From the results presented for cable coupling it can be seen that the important feature is the peaks in the coupling which occur at the frequencies where the tertiary circuit resonates. It, therefore, may be more important to predict the peak coupling at the resonant frequencies than deduce the detail of the coupling. From the equations of cable coupling derived earlier it can be seen that the peaks

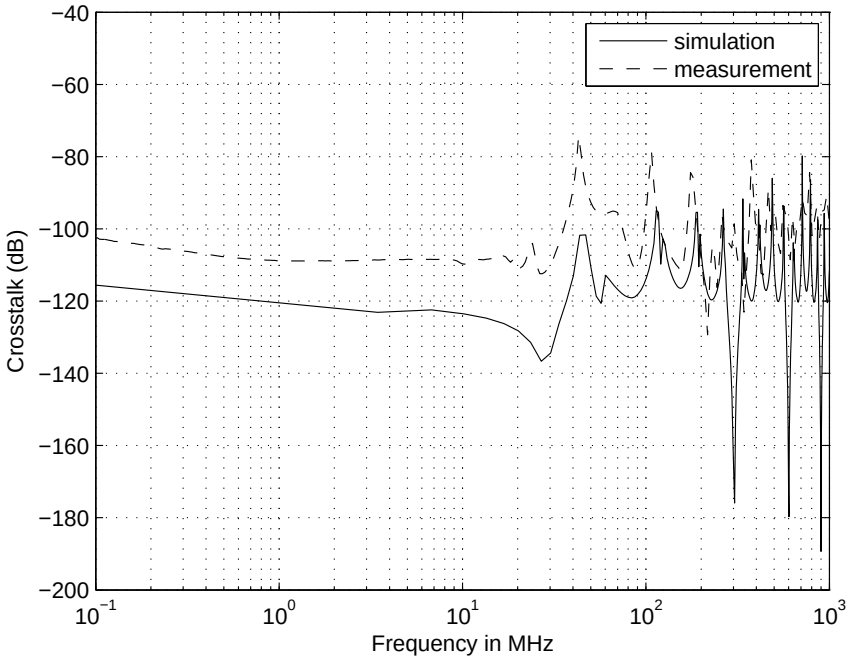

Figure 38: Simulation Crosstalk between a wire and RG214 coax cable compared with measurement (l= 2m, d=5cm, and common connector plates and ground plane, height=touching) using a high frequency model and the Kley model [3] of the transfer impedance.

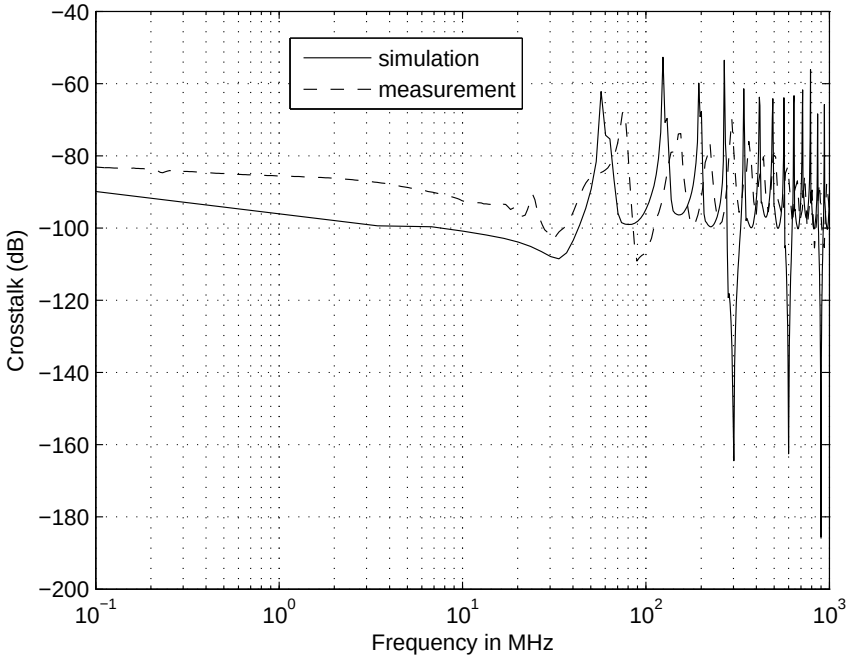

Figure 39: Simulation Crosstalk between a wire and RG214 coax cable compared with measurement (l= 2m, d=5cm and common connector plates, height=10cm) using a high frequency model and the Kley model [3] of the transfer impedance.

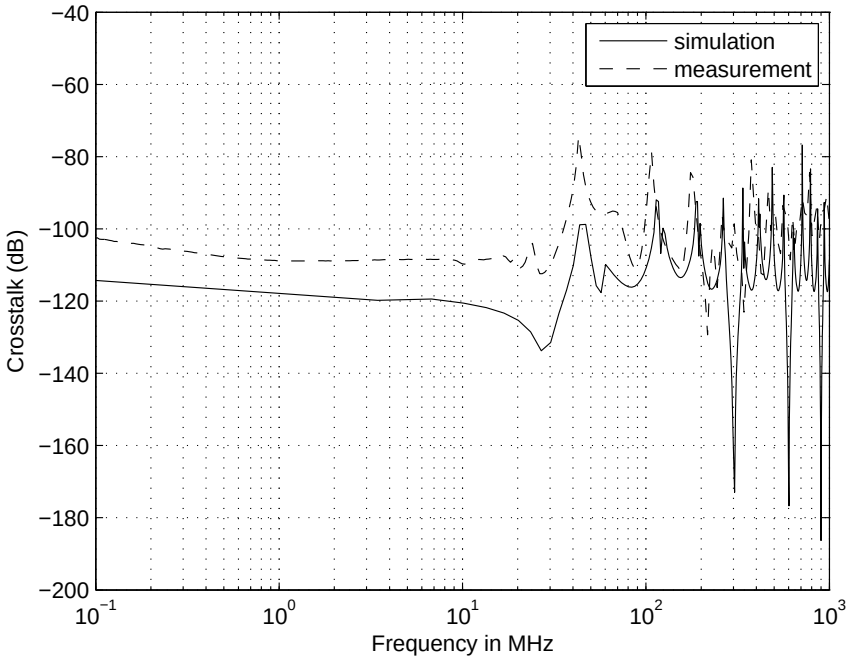

Figure 40: Simulation Crosstalk between a wire and RG214 coax cable compared with measurement (l= 2m, d=5cm and common connector plates, height=touching) using a high frequency model and the Kley model [3] of the maximum expected transfer impedance.

in the cable coupling occur when K_1 and K_2 from (55) and (56)are maximum or for modal propagation when $[K_1]$ and $[K_2]$ from (66) and (67) are maximum . These equations can therefore be used to predict the resonant frequencies of the tertiary circuit. Then by simply calculating crosstalk at the frequencies of resonance of the tertiary circuit a far more useful measure can be derived as Figures 41 and 42. Figures 41 and 42 show measured and predicted cross coupling and the predicted peak coupling at the resonant frequencies for two cables touching or at a 5 cm separation respectively and without a ground plane. It can be seen that the predicted peak coupling provides a far simpler curve and probably more useful.

This approach can also be used for the conditions with a ground plane or in the presence of many parallel cables. However, when there is more than one return path there will be several modes of propagation and each mode needs to be solved for. Figure 43 shows measured and predicted cross coupling and the predicted peak coupling at the resonant frequencies of the two propagation modes (differential and common) for two cables at a 2 cm separation and heights 10cm from the conducting ground plane.

4.4 Statistical analysis of the cable coupling

From the results it can be seen that the cable coupling can be predicted to a reasonable accuracy but that the important parameters may only be poorly known. In this section an method of assessing the degree of coupling in the presence of uncertainty is addressed.

If we consider the case of two cables above ground then the uncertain parameters are the cable height, separation and the terminating impedance of the tertiary circuit (See Figures 3 and 5). For this examination it is assumed that the terminating impedance comprises two parameters: the inductance to ground and the inductance between the two cables (e.g. in Figure 5 for the load end these are Z_{tsvl} for the mutual impedance and Z_{tsl} Z_{tvl} for the impedances to ground) . The parameter values used and their variance are given in Table V. In estimating the variance it was felt that the terminating impedance may only be known within 50% of its assumed value. Therefore initially the effect of these four parameters, assuming they had a uniform distribution, on the peak coupling for the two modes of propagation were plotted and these are given in Figures 44 to 51. Figures 52 and 53 show the results for the separation having a normal distribution, for comparison with Figures 44 and 45.

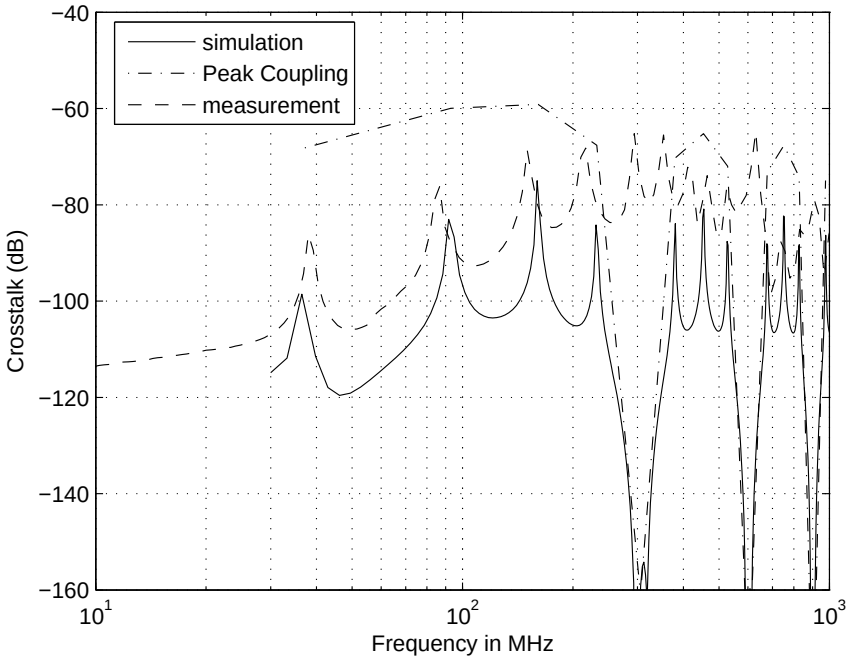

Figure 41: Simulation Crosstalk in two RG58 coax cables compared with measurement (l= 2m, and common connector plates, d=touching) using a high frequency model and the Kley model [3] of the transfer impedance. Also shown is the predicted peak crosstalk at the resonant frequencies

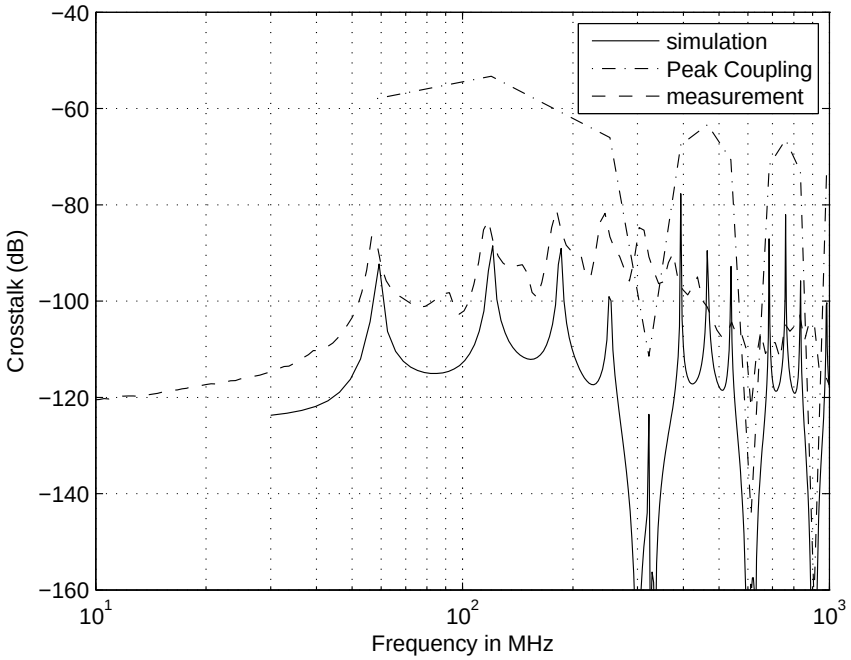

Figure 42: Simulation Crosstalk in two RG58 coax cables compared with measurement (l= 2m, and common connector plates, d=5 cm) using a high frequency model and the Kley model [3] of the transfer impedance. Also shown is the predicted peak crosstalk at the resonant frequencies

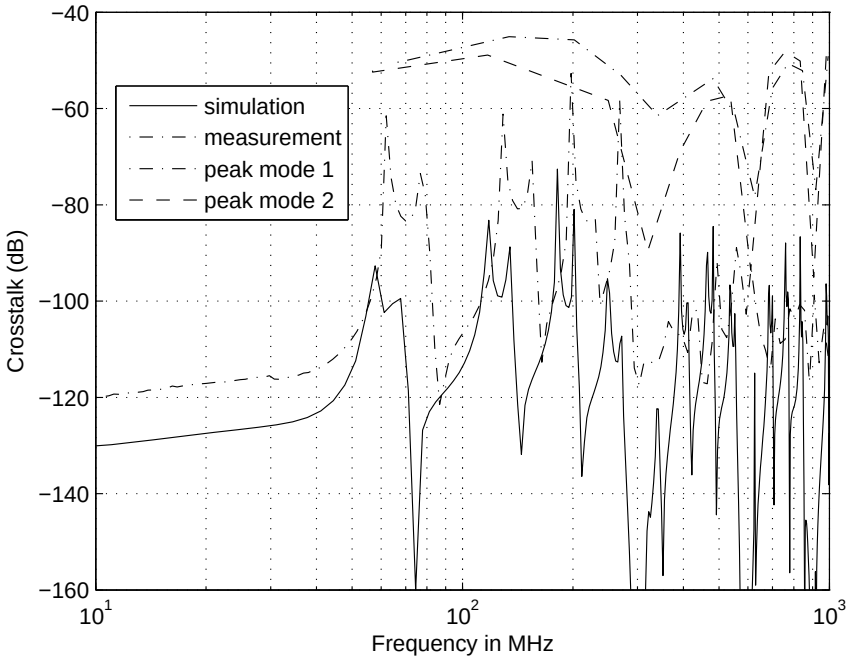

Figure 43: Simulation Crosstalk in two RG58 coax cables compared with measurement (l= 2m, and common connector plates, height=10cm) using a high frequency model and the Kley model [3] of the transfer impedance. Also shown is the predicted peak crosstalk at the resonant frequencies

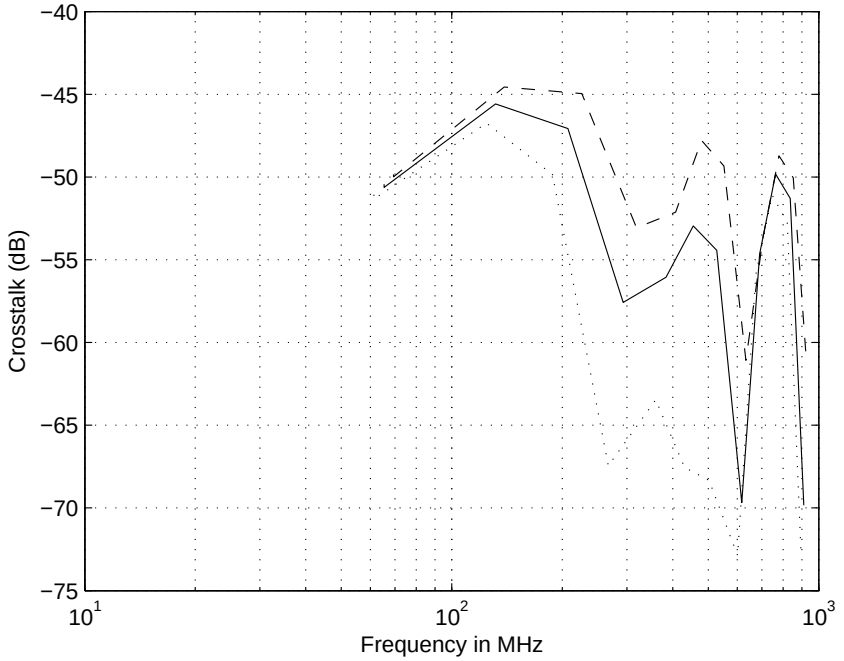

Figure 44: Simulation of the peak Crosstalk in two RG58 coax cables and one standard deviation margin for mode 1 resonant frequencies (l= 2m, and common connector plates, height=10cm) using a high frequency model and the Kley model [3] of the transfer impedance. The terminating inductance between the cables was a variable and had a uniform distribution

Table V Parameters of the variables considered

Variable	**Mean**	**Standard deviation**
Mutual Inductance	0.33 μH	0.16 μH
Inductance to ground	5 nH	2.5 nH
Height	5 cm	2.5 cm
Separation	2 cm	1 cm

From the results presented in Figures 44 to 51 it can be seen that each of the variables have different degrees of impact on the overall results. It can be seen that the terminating inductance to ground does not have a significant effect on the cross coupling. To assess the importance of each of the other parameters the marginal statistical moment of the variance in the cross coupling

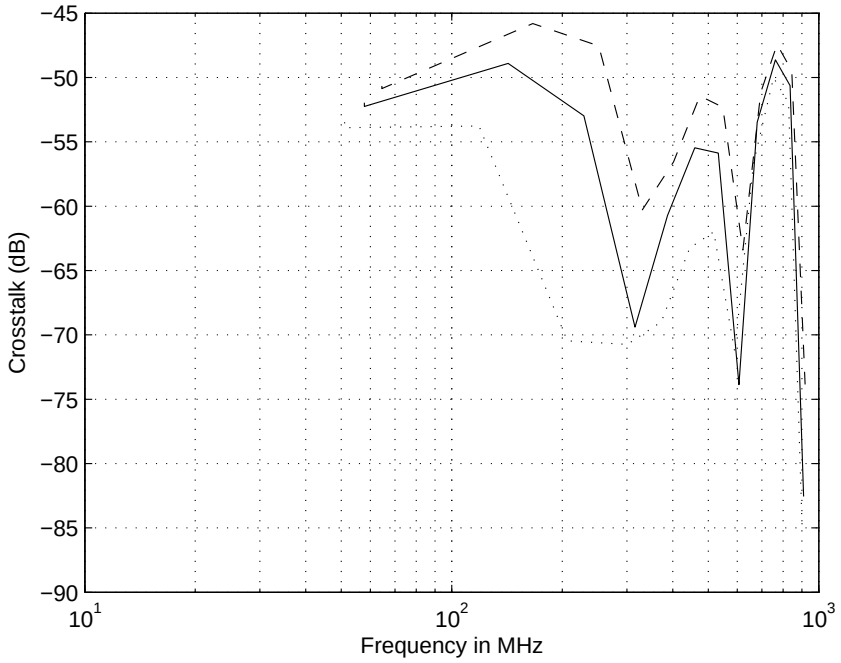

Figure 45: Simulation of the peak Crosstalk in two RG58 coax cables and one standard deviation margin for mode 2 resonant frequencies (l= 2m, and common connector plates, height=10cm) using a high frequency model and the Kley model [3] of the transfer impedance. The terminating inductance between the cables was a variable and had a uniform distribution

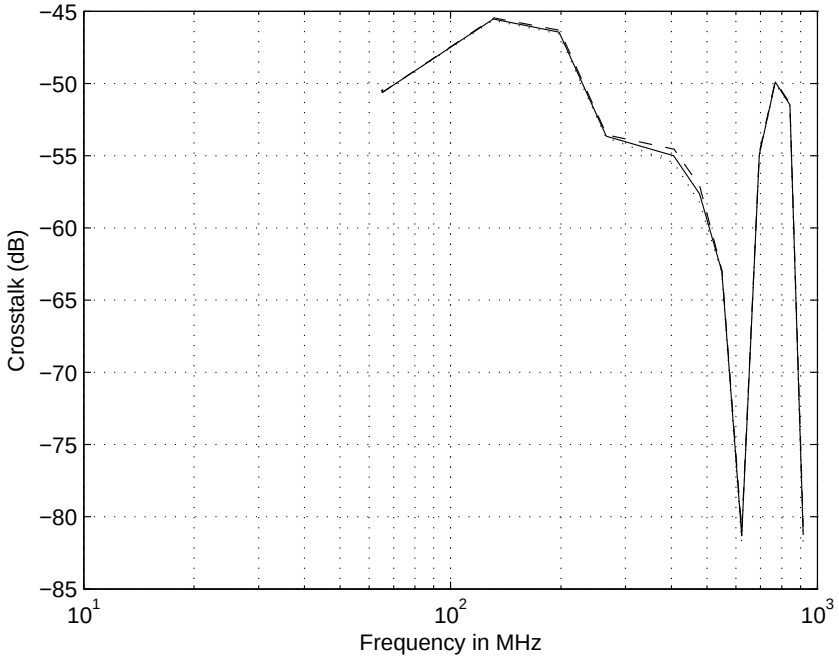

Figure 46: Simulation of the peak Crosstalk in two RG58 coax cables and one standard deviation margin for mode 1 resonant frequencies (l= 2m, and common connector plates, height=10cm) using a high frequency model and the Kley model [3] of the transfer impedance. The terminating inductance between the cables and ground was a variable and had a uniform distribution

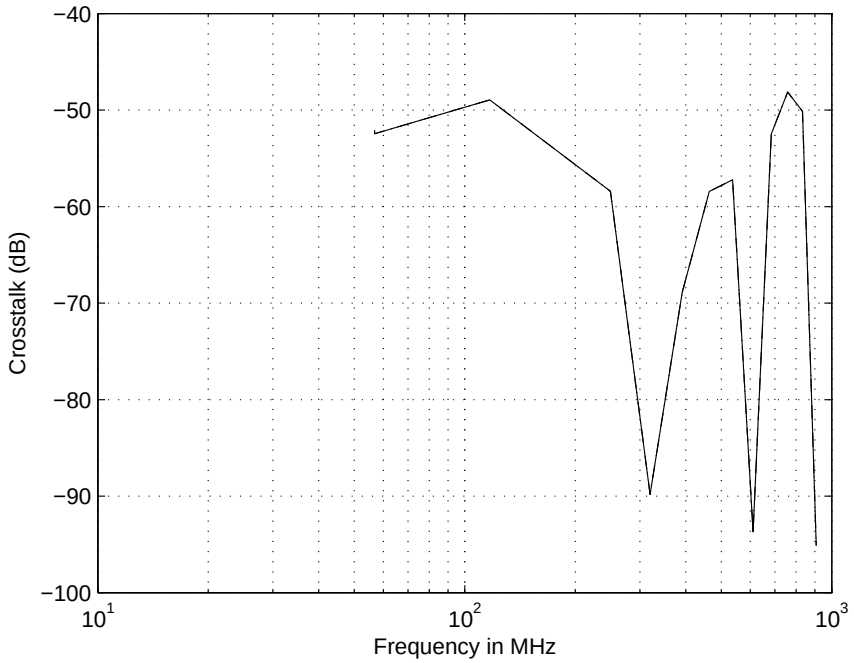

Figure 47: Simulation of the peak Crosstalk in two RG58 coax cables and one standard deviation margin for mode 2 resonant frequencies (l= 2m, and common connector plates, height=10cm) using a high frequency model and the Kley model [3] of the transfer impedance. The terminating inductance between the cables and ground was a variable and had a uniform distribution

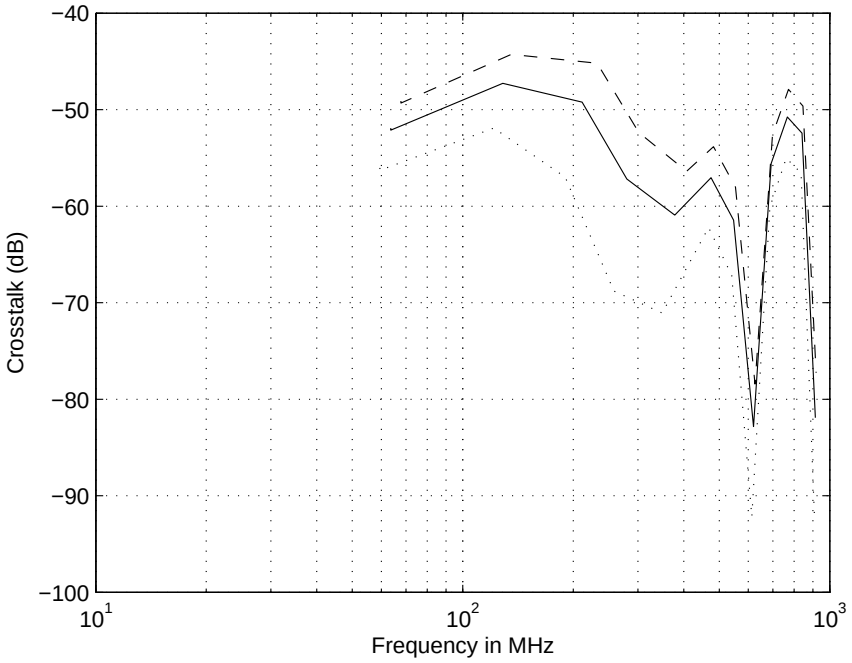

Figure 48: Simulation of the peak Crosstalk in two RG58 coax cables and one standard deviation margin for mode 1 resonant frequencies (l= 2m, and common connector plates, height=10cm) using a high frequency model and the Kley model [3] of the transfer impedance. The height of the cables was a variable and had a uniform distribution

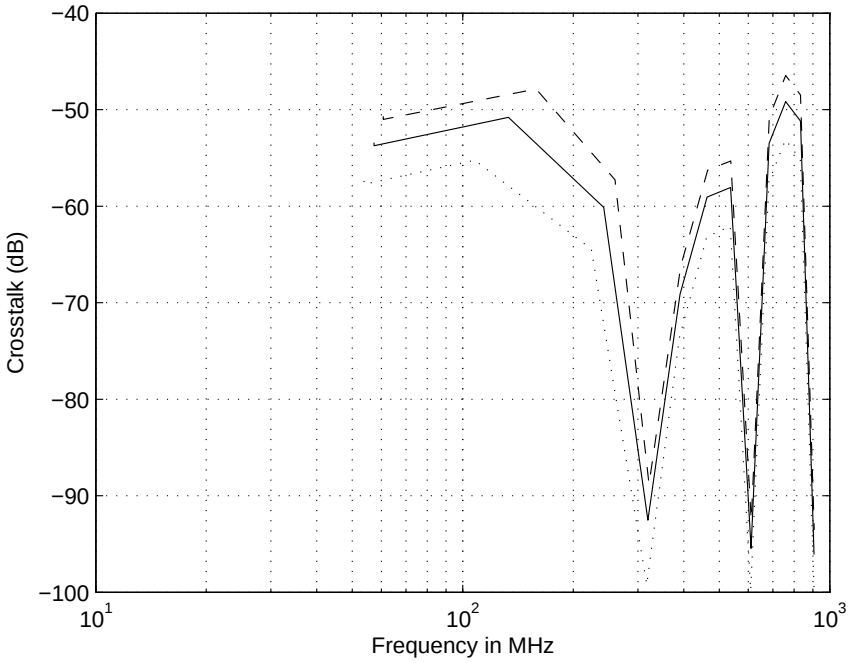

Figure 49: Simulation of the peak Crosstalk in two RG58 coax cables and one standard deviation margin for mode 2 resonant frequencies (l= 2m, and common connector plates, height=10cm) using a high frequency model and the Kley model [3] of the transfer impedance. The height of the cables was a variable and had a uniform distribution

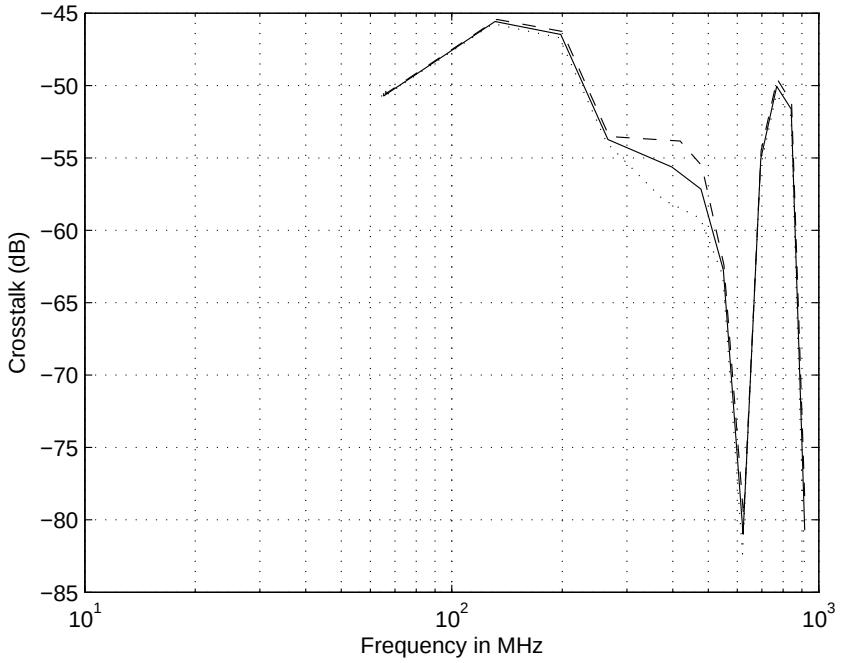

Figure 50: Simulation of the peak Crosstalk in two RG58 coax cables and one standard deviation margin for mode 1 resonant frequencies (l= 2m, and common connector plates, height=10cm) using a high frequency model and the Kley model [3] of the transfer impedance. The separation of the cables was a variable and had a uniform distribution

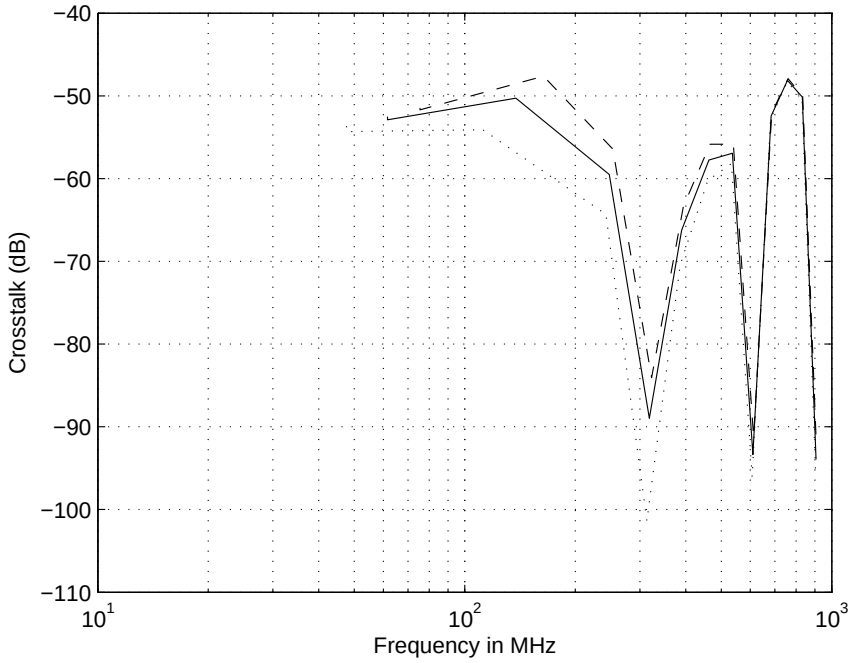

Figure 51: Simulation of the peak Crosstalk in two RG58 coax cables and one standard deviation margin for mode 2 resonant frequencies (l= 2m, and common connector plates, height=10cm) using a high frequency model and the Kley model [3] of the transfer impedance. The separation of the cables was a variable and had a uniform distribution

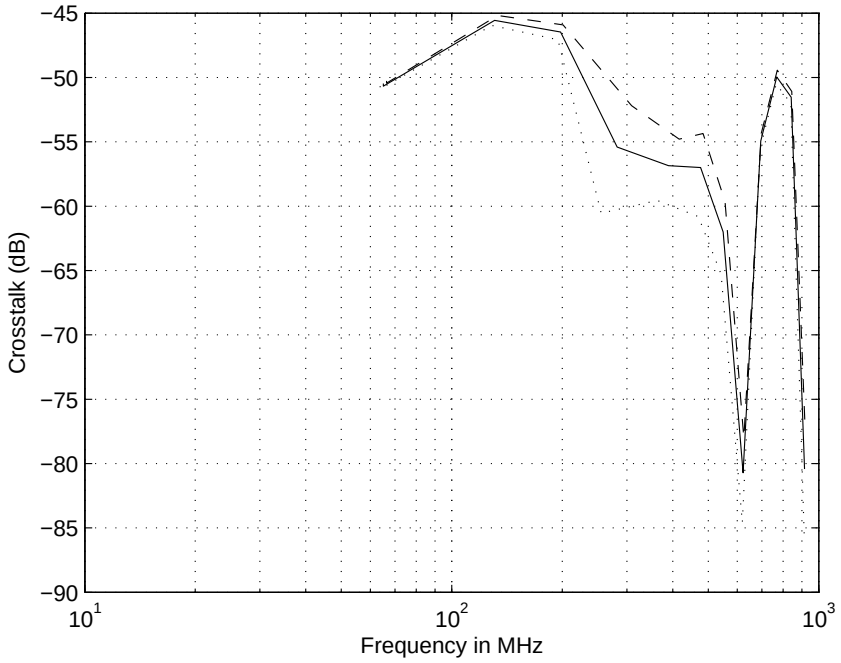

Figure 52: Simulation of the peak Crosstalk in two RG58 coax cables and one standard deviation margin for mode 1 resonant frequencies (l= 2m, and common connector plates, height=10cm) using a high frequency model and the Kley model [3] of the transfer impedance. The terminating inductance between the cables was a variable and had a normal distribution

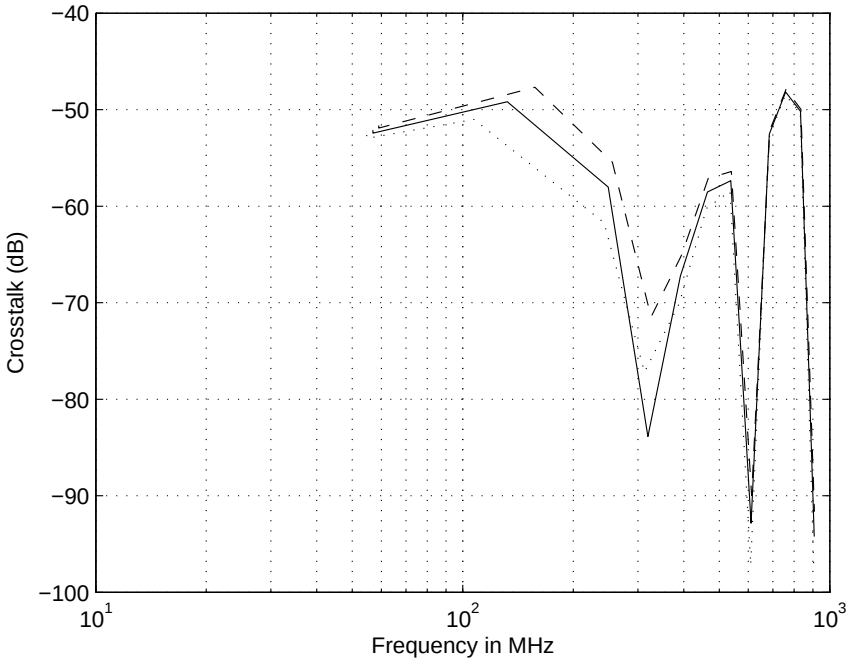

Figure 53: Simulation of the peak Crosstalk in two RG58 coax cables and one standard deviation margin for mode 2 resonant frequencies (l= 2m, and common connector plates, height=10cm) using a high frequency model and the Kley model [3] of the transfer impedance. The terminating inductance between the cables was a variable and had a normal distribution

peak amplitude and frequency for the other three variables were calculated using (86) and the results are given in Table VI. Table VI provides a useful incite into the importance of each of the parameters.

Table VI Marginal statistical moment of the parameter variances

Variable	**Frequency**		**Amplitude**	
	Common mode	**Differential mode**	**Common mode**	**Differential mode**
Mutual Inductance	0.38	0.8	0.3	0.74
Height	0.58	0.027	0.64	0.015
Separation	0.013	0.16	0.001	0.2

The results presented in Table VI shows that the height of the cables has an important influence on the maximum cable coupling but only at frequencies associated with the common mode. This is because the height effects the common mode propagation impedance. Similarly the separation of the cables has a much small impact and mainly effects the differential mode resonant frequencies. This is also as expected as the differential mode propagation characteristics are mainly effected by the separation. The mutual inductance of the terminating impedance also strongly effects the cable coupling but mostly at the resonant frequencies of the differential mode.

5 Conclusions

Good progress has been made in developing a model for coaxial cable coupling. Both single braided cables and double braided cables were investigated. The cable layouts considered were either with a ground plane or without a ground plane. The models produced provided reasonable agreement with the measurements provided. The cable coupling is strongly effected by parameters such as cable height, separation and stray impedances all of which have a large variation in a normal cable layout. Therefore practical ways of deducing the cross coupling were investigated such as a simplified representation and non deterministic solutions.

For a practical approaches for estimating cable coupling it was found that the maximum cable coupling can be estimated from the coupling amplitude of the resonant frequencies. The actual frequencies may be very variable so it is not valuable to find the detail of the cable coupling variation with frequency but it is more practical to simply plot along the maximum coupling at the resonant frequencies.

A non deterministic approach for estimating the cable coupling was also investigated. It was shown that the range amplitude in cable cross coupling could be estimated and also the importance of each of the parameters could also be demonstrated.

This work is only touched on analyzing the measurement data provided and there is a lot more work which can be done. There is probably at leat a couple

publishable papers from the work done so far. It is hoped that in the near future future studies can include the following.

- An estimate of probability function and the cumulative probability function to enable optimized cable layout
- Power cable coupling
- Twisted pair
- Multiple cable coupling
- Different screens and cable trunking

Appendix

cable parameters

Cable type	N	n	D_0 /mm	d /mm	l /mm	α
RG58	12	9	2.95	0.127	19.79	27.42
RG58-A	16	7	2.95	0.127	19.72	27.56
RG58-Rep	18	6	2.95	0.127	19.79	27.56
RG214 (I)	24	6	7.42	0.16	18.36	52.9
RG214 (O)	24	7	8.05	0.16	19.79	53

The RG58 and RG58-A parameters are from [5] and the RG58-Rep N and n parameters were provided by [7] with the rest taken from RG58-A

comparison of nomenclature

This Report	Kley [3]	Vance [1]	Report [7]
P	-	P	-
N	m	$\mathcal{C}$	ζ
n	n	N	N
d	d	d	d
α	α	α	ψ
D_m	D_m	$2a$	$2b$
χ	B	K	χ
F	G	F	F
k_1	k_1	-	k
k_2	k_2	-	k
D_l	D_L	-	D_l
D_g	D_G	-	D_g

References

[1] E.F. Vance , *Shielding Effectiveness of braided-wire shields*, IEEE Trans. EMC, Vol 17, No. 2, 1975, pp 71-77.

[2] M. Tyni , *The transfer impedance of coaxial cables with braided conductors*, Proceedings of EMC symposium, Wroclow, Poland, Sept. 1976, pp 22-24.

[3] T. Kley , *Optimized single-braided cable shields*, IEEE Trans. EMC, Vol. 35, No. 1, 1993, pp 1-9.

[4] J.N. Katakis , *Transfer impedance of wire braided coaxial cables at radio and microwave frequencies*, MEng thesis, University of Sheffield, Feb. 1983.

[5] E.F. Vance , *Coupling to shileded cables*, 1978, Pub. A Wiley, ISBN 0-471-04107-6

[6] D.R.J. White and M Mardiguian, *A handbook series on EMI and Compatibility, Volume 3: Electromagnetic shielding*, 1988, Pub. Don White Consultants Inc., ISBN-13:978-0944916031

[7] J-C. Aldon, S. Antipolis and F. Leferink, *Transfer impedance of cables*, report 3.3 RCTR study 1997.

[8] F.A. Benson, P.A. Cudd and J.M. Tealby, *Leakage from coaxial cables*, IEE Proc-A, Vol. 139, No. 6, 1992, pp 285-303.

[9] S. Sali *Response of externally excited coaxial cables with wire braided shields*, IEE Proc. Sci. Meas. Technol., Vol 141, No. 4, 1994, pp 266-272

[10] S. Sali *A Circuit based approach for crosstalk between coaxial cables with optimum braided shields*, IEEE Trans. EMC, Vol 35, No. 2, 1993, pp 300-311.

[11] L de Menezes, D W P Thomas and Christos Christopoulos, *Accounting for Uncertainty in EMC studies*, submitted to esa 2009.

[12] S. J. Julier and J. K. Uhlmann, *Unscented filtering and nonlinear estimation*, Proc. IEEE, Vol. 92, No. 3, March 2004 pp 401-422.

[13] J. Zhang, *The calculation of formulae, and experimental methods in error propagation analysis*, IEEE Trans. on Reliability , Vol. 55, No. 2, June 2006 pp 169-181.

[14] E W Wiesstien, *Gaussian Quadrature*, MathWorld–A Wolfram Web Resource (July 2007), http:mathworld.wolfram.com/GaussianQuadrature.html.

[15] L de Menezes, A Ajayi, C Christopoulos, P Sewell and A Borges, *Efficient computation of stochastic electromagnetic problems using unscented transforms*, IET Science, Measurement and Technology, Vol. xx, No. 2, 2008 pp 88-95.

[16] A. Papoulis, *Probability, Random Variables, and Stochastic Processes*, 3rd Ed. Pub. New York: McGraw-Hill, 1991.

[17] L. Korteweg *Crosstalk in cables*, Internship report, Thales Nederlands B.V., January 2008.

[18] T. Wijnands *Analysis Report: Crosstalk in cables*, Thales Nederlands B.V., July 2008.

[19] Filotex *Computer wires and cables*, Issue 83, Modif 86, Pub. Filotex, 140-146 Rue Eugene Delacroix, 92120 Dravel France.

[20] Suhner *Jumperkabel Fur Den mobilfunk, Techische Daten*, Pub. Huber+Suhner AG, Mehlbeerenstr. 6, 82019 Taufkirchen.